ISTANBUL TECHNICAL UNIVERSITY ★ GRADUATE SCHOOL OF SCIENCE ENGINEERING AND TECHNOLOGY

FABRICATION AND CHARACTERIZATION OF A HELICOPTER COMPOSITE TAIL CONE

M. Sc. THESIS

Deniz KAVRAR

Deparment of Metallurgy and Materials Engineering

Materials Engineering Programme

AUGUST 2012

ISTANBUL TECHNICAL UNIVERSITY ★ GRADUATE SCHOOL OF SCIENCE ENGINEERING AND TECHNOLOGY

FABRICATION AND CHARACTERIZATION OF A HELICOPTER COMPOSITE TAIL CONE

M. Sc. THESIS

Deniz KAVRAR
506091428

Deparment of Metallurgy and Materials Engineering

Materials Engineering Programme

Thesis Advisor: Prof. Dr. M.Lütfi ÖVEÇOĞLU

AUGUST 2012

İSTANBUL TEKNİK ÜNİVERSİTESİ ★ FEN BİLİMLERİ ENSTİTÜSÜ

BİR HELİKOPTER KOMPOZİT KUYRUK KONİSİ İMALATI VE KARAKTERİZASYONU

Yüksek Lisans Tezi

Deniz KAVRAR
506091428

Metalurji ve Malzeme Mühendisliği

Malzeme Mühendisliği Bölümü

Tez Danışmanı: Prof. Dr. M.Lütfi ÖVEÇOĞLU

AĞUSTOS 2012

Deniz Kavrar, a **M.Sc.** student of ITU **Institute of Science and Technology** student ID 506091428, successfully defended the **thesis** entitled "Fabrication and Characterization of a Helicopter Composite Tail Cone", which she prepared after fulfilling the requirements specified in the associated legislations, before the jury whose signatures are below.

Thesis Advisor :	**Prof. Dr.M.Lütfi ÖVEÇOĞLU** İstanbul Technical University	.....
Co-advisor :	**Assoc.Prof.Dr.Halit S. TÜRKMEN** İstanbul Technical University	.....
Jury Members :	**Assoc.Prof.Dr. Burak ÖZKAL** İstanbul Technical University	.....

Date of Submission : 4 May 2012

Date of Defense : 24 August 2012

To my family,

FOREWORD

I would thank to my supervisor Prof.Dr. M.Lütfi ÖVEÇOĞLU. I would also thank to Assoc.Prof.Dr.Halit S.TÜRKMEN sincerely for his support, guidance and encouragement. Additionally, I would thank to Aytekin Güven and Müslüm Çakır for helping me during this thesis.

Family is always very important for us to be successful in any subject. For this case, I would like to thank my Family for their endless supports.

August 2012

Deniz KAVRAR

Metallurgy and Materials Engineer

TABLE OF CONTENTS

Page

ABBREVIATIONS

DSC **:** Differential Scanning Calorimetry
FRP **:** Fiber Reinforced Polymer
MMC **:** Metal Matrix Composite
RTM **:** Resin Transfer Molding
SMC **:** Sheet Molding Compound

LIST OF TABLES

Page

LIST OF FIGURES

Page

FABRICATION AND CHARACTERIZATION OF A HELICOPTER COMPOSITE TAIL CONE

SUMMARY

This thesis presents manufacturing an unmanned helicopter composite tail boom and associated with mechanical tests. The tail boom effectively couples two masses together; the main rotor and the tail rotor. These each constitute both static and dynamic forces. Because it is long to obtain the enough distance between the tail rotor and the main rotor, the materials used for manufacturing the tail boom needs to be a lightweight material. A hand lay-up technique is used for the manufacturing of the tail booms. Primarily, two different conical shells were produced with hand lay-up technique. One was produced with 3-ply carbon fiber. To increase the resistance of the shell to torsion, it was strengthened by stiffeners. The other one was produced using honeycomb as core material and carbon/epoxy face sheets. The tail boom was also modeled by using ANSYS finite element software and static analyses were achieved. In test results, bending and torsional-bending features of manufacturing with honeycomb between 2-ply carbon fiber were better than manufacturing with 3-ply carbon fiber with stiffeners. Therefore, an unmanned helicopter tail boom was manufactured with honeycomb between carbon fiber. Totally, four plies carbon fiber and carbon fiber was used for unmanned helicopter tail cone. Cut four plies carbon fiber was weighed. In this process, the woven carbon (280 grams per square meter) was used in this production. Also, 2mm honeycomb was used for this process. 700 grams epoxy/hardener mixture was prepared for 700 grams composite materials. 500 g epoxy was mixed with 200 g hardener. The experiments had been repeated for 5mm, 10mm, 15mm and 20mm bending and torsional-bending displacements. Helicopter tail boom had been created a model using with ANSYS software and then, it had been solved for each displacements. Experimental and static analysis results had been compared with each other. Also, different tail cones had been created by using ANSYS finite element software.

Furthermore, the result of DSC analysis is compatible with technical information of Hexion L285 epoxy. According to DSC analysis in İTÜ Polymer Laboratory, the glass transition event, T_g, is observed at 0 °C as an exothermic stepwise increase. The endothermic peak temperature reflects the maximum rate of curing of the resin. The endothermic peak temperature is 58.45° C.Therefore, composite semi-conical shells must be produced in 60ºC.

Also, carbon fiber composite material was analyzed with Bruker D8 Advance X-ray diffractometer in İTÜ. According to İTÜ PML Laboratory, XRD diffraction study is similar to previous studies. Carbon fiber composite diffraction degree is approximately 26º.

BİR HELİKOPTER KOMPOZİT KUYRUK KONİSİ İMALATI VE KARAKTERİZASYONU

ÖZET

Bu çalışmanın amacı karbon fiber kompozit malzeme ile üretilmiş bir helikopter kuyruk konisinin mekanik ve kimyasal özelliklerini incelemektir. Kompozit malzemenin havacılık sektöründe sıklıkla tercih edilmesinin en önemli sebebi mukavemet/ağırlık oranının yüksek olmasıdır.

Havacılık ve uzay teknolojisinde yapılan yenilikler, araştırma geliştirme programlan, tüm dikkatleri, yüksek dayanımlı, hafif ve kolayca denetlenip istenilen yönde ayarlanabilen mekanik özelliklere sahip, takviyeli plastik malzemeler üzerinde yoğunlaştırılmıştır. Hafiflik, güçlülük, uçuş menzilinin ve yük kapasitesinin artması, hizmet süresinin uzun olması korozyon direnci, bakım onarım imkânı ve uygulamaya konulacak teknik yenilikler bakımından kompozit malzemeler, askerî ve sivil uçaklarda giderek artan oranlarda kanat, gövde, yatay/dikey dengeleyiciler, helikopter pervane ve milleri ve diğer bölümlerde yaygın olarak kullanım alanına girmişlerdir.

Bu çalışmada bir insansız hava aracı için tasarlanan kuyruk konisi polimer matrisli kompozit malzemeden üretilmiştir. Karbon fiberle güçlendirilmiş epoksi matrisli kompozit malzeme kuyruk konisi üretimi için kullanılmıştır. Ayrıca çift yönlü karbon fiber arasına bal peteği kullanılmıştır.

Orijinal kuyruk konisi üretimi yapılmadan önce iki farklı özellikte modeller yapılmıştır. Modellerin boyutu yaklaşık olarak 50 cm olup yarı konik yapıdadır. Yapılan modellerden biri 3 kat karbon fiber ve 16 cm aralıklarla konulan 4 kat karbon fiberli yapı, diğeri ise 2 kat karbon fiber arasına bal peteği ile güçlendirilmiş yapılardır. İki farklı model kuyruk konisinde yapılan deneyler sonucunda daha iyi eğilme ve eğilmeli burulma özelliği gösteren bal petekli yapının orijinal kuyruk konisi üretimi için uygun olduğu tespit edilmiştir. Ayrıca 2 kat karbon fiber arasına bal peteği ile güçlendirilen yarı konik yapının daha hafif olduğu tespit edilmiştir. Hafiflik havacılık sektörü için önemli bir özellik olduğundan dolayı dikkate alınmıştır.

Model ile elde edilen bilgiler dahilinde orijinal kuyruk konisi 4 kat karbon fiber ve bal peteği yapısı kullanılarak üretilmiştir. Orijinal kuyruk konisi için 150 cm boyunda tahta kalıp kullanılmıştır. Karbon fiber yapının yüzey pürüzlülüğünün olmaması ve kür sonrası kalıptan kolay ayrılması amacıyla üretim yapılmadan kalıp iç yüzeyine vaks sürülmüş ve bir süre beklenmiştir. Vaksın kuruması ile birlikte orijinal kuyruk konisi üretimi için kalıba uygun şekilde karbon fiberler kesilmiştir. Kesilen 4 kat karbon fiber tartılmış ve 700 g ağırlığında olduğu tespit edilmiştir. Karbon fiber ağırlığına eşdeğer sertleştirici/reçine karışımı hazırlanmıştır.

Sertleştirici/reçine karışım oranı 2/5 alınmıştır. Karışım oranına göre 200g sertleştirici ile 500 g reçine homojenite sağlanana kadar karıştırılmıştır. Orijinal kuyruk konisi yapımında 2 kat karbon fiber yeterli miktarda reçine/sertleştirici karışımı ile ıslatılmıştır. Daha sonra 2mm kalınlığında bal peteği serilmiştir. Bal peteğinin boşluklu yapıda olmasından dolayı fazla ağırlık oluşturmaması için sertleştirici/reçine karışımı bal peteği üzerine sürülmemiştir. Bal peteğinin üzerine tekrar 2 kat karbon fiber serilmiştir. Bu şekilde kalıba elle yatırılan kompozit, naylonun kenarlarına sızdırmazlık bandı ile yapılan vakum torbası içine alınmıştır ve basınç yaklaşık 650 mbar ve sıcaklık yaklaşık 55^{o}C'de 24 saat kürlenmiştir. Aynı şekilde kuyruk konisinin diğer yarısı da üretilip yeterli miktarda sertleştirici/reçine karışımı ve karbon bandı ile üretilen yarı konik yapılar birleştirilmiştir. Karbon fiber bandın uygulanacağı kısımlar taşlanarak pürüzlü bir yüzey yapılmıştır. Bu sayede karbon bandın konik kabuğa yapışma özelliği arttırılmıştır. Kullanılan karbon bandı 5cm genişliğinde olup içten ve dıştan olmak üzere 2 kat uygulanmıştır. Daha sonra ise hem iç hem dış taraftan geçirilen vakum torbası ile tekrar kür edilmiştir. Yeniden kürleme işleminde ısıtma kullanılmamış olup sadece 650 mbar vakum uygulanmıştır.

Ana rotorun oluşturduğu momente karşılık helikopter gövdesi zıt yönde dönme eğilimi gösterir. Bu nedenle dengeyi sağlamak amacıyla kuyruk rotoru ana rotorun ters yönünde dönmektedir. Bu nedenle kuyruk konisi üzerinde eğilmeli burulma yükü meydana gelir. Ayrıca kuyruk konisinin ağırlığından kaynaklanan eğilme meydana gelmektedir. Bu nedenle, kuyruk konisi üzerinde eğilme ve eğilmeli burulma özellikleri incelenmiştir.

Deneyler yer değiştirmeye göre yapılmış olup her bir deney üç kez tekrarlanmıştır. Üretilen kuyruk konisi için 5mm, 10mm, 15mm, 20mm için eğilme ve eğilmeli burulma deneyleri yapılmıştır. Deneyler istenilen yer değiştirme değerlerine ulaştıktan sonra deneyin başladığı noktaya geri dönmüştür. Deney sonuçlarına göre kuvvet-yerdeğiştirme grafikleri çizilmiştir. ANSYS sonlu elemanlar analiz programı ile kuyruk konisi oluşturulmuş ve deney düzeneğinde yer alan ankastreler modellenmiştir. Analiz programı için karbon fiber, bal peteği ve çelik malzemelerin mekanik özellikleri tanımlanmıştır. Daha sonra ise yapıda düzgün bir ağ oluşturulup yer değiştirmeye göre çözüm yapılmıştır. ANSYS sonlu elemanlar analiz programı ile deney düzeneğinden elde edilen veriler karşılaştırılmıştır.

Ayrıca üretilen kompozit malzeme için diferansiyel taramalı kalorimetri (DSC) ile epoksinin kürleşme özellikleri incelenmiştir.

Camsı geçiş sıcaklığı polimer esaslı malzemeler için ayırt edici bir özelliktir. Malzemenin camsı özelliğini kaybedip viskoz özellik kazandığı sıcaklık olarak tanımlanır. Her zaman polimer esaslı malzemenin erime noktasından daha düşük sıcaklık değerlerindedir. Diferansiyel taramalı kalorimetri (DSC) termal analizde kullanılan termoanalitik bir yöntemdir. DSC eğrileri numune entalpisinin zamana göre değişiminin sıcaklığa karşı değişen grafikleridir. DSC analizi ile parçanın ısıtılması soğutulması ve eş sıcaklıkta tutulmasıyla oluşan enerji farklılıklarındaki değişimi analiz edilir. Enerji farklılıklarıyla numunede nicel olarak gözlenen hal değişimi ve de oluştuğu noktalarda sıcaklığın bulunmasına ve ayrıca erime sürecine bağlı olarak malzemenin karakterizasyonuna ait bilgiler edinilir. Termoset bir polimer olan epoksi 10°C/dak. hızında 0°C'den başlanılarak 160°C'ye kadar ısıtılmıştır. İlk endotermik pik 0°C'ye yakın bulunmuştur. Kürleşmemiş epoksinin camsı geçiş sıcaklığına denk gelmektedir. Zamanla sıcaklıktaki artış sonucu DSC

analizinde 58.45°C'de endotermik pik oluşmuştur. Bu sıcaklık sonrasında malzeme kürleşmiştir. Kürleşme ile birlikte epoksinin camsı geçiş sıcaklığı sonsuza doğru kayma göstermiştir. L285 Hexion epoksinin literatürde verilen kürleşme sıcaklığı ise 60-65°C'dir.

Ayrıca karbon fibere göre XRD paterni çekilmiştir. İTÜ Toz Metalürjisi Laboratuarı'nda yapılan çalışmaya göre karbon fiber kompozit malzemesinin maksimum pik derecesi 26°'de görülmüştür.

1. INTRODUCTION

Carbon fiber reinforced advanced composite materials are being used for a variety structural applications because of their useful mechanical properties, including high strength-to-weight ratio and corrosion resistance [1].The use of composite industries is highly prevalent today because of the enormous benefits they offer in our lives, society, and environment [2].The aerospace industry was among the first to realize the benefits of composite materials. Airplanes, rockets, and missiles all fly higher, faster, and farther with the help of composites.

In the past decade, significant use has been made of polymer matrix composites as structural materials for airframes in both military and civilian applications [3]. Helicopters in particular have seen remarkable growth in the number of components now manufactured using fiberglass, carbon, or aramid (Kevlar) fibers. But then, rotary-wing aircraft have always had a closer relationship to composite materials than their fixed-wing counterparts.

Advanced polymer composites generally contain reinforcing fibres in the form of continuous filamentary tows or fabrics and properly formulated polymetric matrices. Structural adhesives (mostly in the form of supported or unsupported film) and honeycomb cores are also used for making sandwich structures and metallic laminates.

One of the uses of polymer matrix materials is for the tail boom of helicopters. Today, most of the helicopter tail cones are made of carbon fiber reinforced composite materials. Thus, the weight of the helicopters has been reduced with the use of composite materials. For this reason, aviation industry has been developed day by day. So, today many researchers have been conducted on the use of the composite materials in aerospace industry.

In this thesis, helicopter tail cone which is produced with carbon fiber reinforced epoxy composite materials has been investigated properties of bending and torsional

bending. Experimental results have been compared with static analysis. Furthermore, differential calorimetry analysis has been performed for carbon fiber reinforced epoxy composite materials.

1.1 Background

Although fixed-wing aircraft receive all the attention by most historians, helicopter flight was the first flight envisioned by man. In fact, the ancient Chinese were playing with a hand-spun toy that rose upward when revolved rapidly and as early as the mid 1500's, the great Italian Leonardo Da Vinci had used his fertile mind to make drawings of a machine that we now know as the helicopter. Many extraordinary models were developed by an ever increasing number of great thinkers, but all the pioneers were missing two essentials: a true understanding of the nature of lift and an adequate engine [4].

The great breakthrough came at the end of the nineteenth century. The internal combustion engine made it possible for the pioneers to develop full-sized models with an adequate power source. It was then they found the first of many great problems: torque, the effect produced by the rotor to force the fuselage to rotate in the opposite direction as the engine [4].

The beginning of the 20th century saw the pioneers experimenting and resolving many of the problems that appeared with each advancement. The old saying, “One step forward and two steps back," was the order of the day for the early pioneers. Dissymmetry of lift, the action that tended to cause the early helicopters to flip over, confounded the early pioneers until the invention of the swash plate. The swash plate, with cyclic pitch control allowed the rotor blade angles to be altered so that lift would be equal on each side of the central shaft [4].

However, there were many problems that had not been worked out on any one individual helicopter. Then on November 13, 1907, the French pioneer Paul Cornu lifted a twin- rotored helicopter into the air entirely without assistance from the ground for a few seconds. After that, several models were produced by many designs but there were no more great advances until another French pioneer, Etienne Oehmichen, became the first to fly a helicopter a kilometer in a closed circuit in

1924. It was a historic flight taking 7 minutes and 40 seconds. Advances began to come fast and furious. One of the more important advances in the development of vertical flight was made by the Spaniard Juan de la Cierva. His design, called the autogyro, was not a true helicopter but his contribution was very important. By 1936, many of the problems had solutions and with the introduction of the German Focke-Wulf Fw 61, the first practical helicopter was a reality. Vertical flight was not a dream anymore [5].

In this century, development of high performance structures and components in advanced materials is critical with reduced material and production costs. The use of composites in the aerospace industry has increased dramatically since the 1970s. Traditional materials for aircraft construction include aluminum, steel and titanium. The primary benefits that composite components can offer are reduced weight and assembly simplification. The performance advantages associated with reducing the weight of aircraft structural elements has been the major impetus for military aviation composites development. Although commercial carriers have increasingly been concerned with fuel economy, the potential for reduced production and maintenance costs has proven to be a major factor in the push towards composites. Composites are also being used increasingly as replacements for metal parts on older planes. Figure 1.1 shows current and projected expenditures for advanced composite materials in the aerospace industry [6].

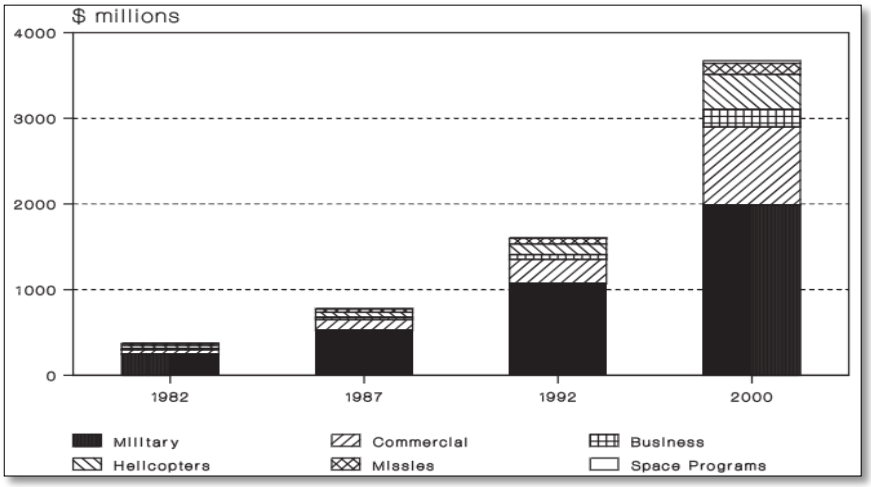

Figure 1. 1: Advanced composite sales for the aerospace industry [6].

The use of aluminum alloys for aerospace platforms has developed over the past 75 years following initially a high specific strength route based on a high copper alloying content (2000 series) and a high zinc alloying content (7000 series). In parallel, heat treatments were developed to improve and optimize the balance between ultimate and yield strengths, ductility, resistance to the growth of fatigue cracks, toughness and resistance to corrosion. Because of their differing characteristics, the 2000 series have been predominantly used for fuselage skins and lower wing surfaces, whilst the 7000 series have been used for upper wing surfaces, spars and ribs, in sheet, plate and extrusion forms [7].

The use of steel is relatively limited, at about 7% of the airframe structure. Steels are used where the structure requires very high strength and resistance to elevated temperature or where space is restricted. Primarily use of steels is in pylon structure, landing gear and slat track components, plus some small standard parts such as bearings, springs, bolts band washers [7].

Titanium alloys are used in current airframe applications for medium-sized forgings in high load transfer components such as the engine pylon and undercarriage support fittings on the wing, composite component joints and bolts. Those components which can be produced effectively by superplastic forming/diffusion bonding such as engine pylon secondary structure and lower wing unloaded manhole doors are also in production. Superplastic forming/diffusion bonding has been pursued for use on other components, and demonstrators have been manufactured for spoilers, ailerons, flap beams and fuselage sections. However, to date, none of these applications has proved to be attractive to current project teams when evaluated against the drivers of cost and performance, and the technology may be in waiting for applications on supersonic platforms, where the basic material properties bring greater benefits.

Today, composite materials are preferred instead of traditional materials for their high performance properties. Especially metal matrix, polymer matrix and ceramic matrix composites are commonly used in aerospace industry. Table 1.1 is shows that mechanical properties of some common metals and fibres.

Table 1. 1: Comparison of specific moduli of some common metals and fibres [8].

Materials	Specific gravity	Young's modulus (GPa)	Specific modulus (GPa)
Steel	7.9	200	25.3
Aluminium	2.7	76	28
Titanium	4.5	116	25.7
Glass (bulk and fibre)	2.5	72	27.6
Carbon (high strength fibre)	1.8	295	164
Kevlar 49 fibre	1.45	135	93

1.2 Literature Review

The tail boom must provide structural support for the tail rotor, the fin and the tail plane, as well as having some aerodynamic characteristics. A tail boom which is a smooth continuation of the hull will have lower drag in forward flight than the 'pod and boom' construction. However, a wide tail boom will suffer a greater download in the hover [9].

A streamlined tail boom may be practical on an executive transport, but for other purposes rear loading ramps or clamshell doors may be needed and these always result in a hull having higher drag. The boom has to be high set and slim to give clearance for rear loading [9].

The tail boom effectively couples two masses together; the main rotor and the tail rotor. These will each experience different forces, some static and some alternating. The main rotor will apply vibrations to the hull, but the tail rotor will tend to lag behind because of its mass and the result will be stress on the tail boom. Figure 1.2.(a) shows that when starting, whirling forces from the main rotor will rock the hull from side to side. A tail rotor mounted atop the tail fin will resist the rocking and place the tail boom in torsion. The mass of the tail and the torsional stiffness of the boom will create a resonant system and if the resonant frequency coincides with an exciting frequency the tail assembly will oscillate in torsion. If torsional oscillation results from a flight frequency, the resonant frequency will have to be changed. Intuitively, stiffening the tail boom would do this, but weakening it would also change the resonant frequency to a lower value. A lengthwise slot in the skin of a tail

boom will reduce the torsional oscillation frequency without materially altering the bending stiffness. Damping material may be placed across the slot where it will be highly effective. Figure 1.2(b) shows that main rotor whirling in the foreand- aft direction subjects the tail boom to bending loads as does tail rotor imbalance. Again a resonance may be present. The Robinson R-22 passes through some quite noticeable tail boom bending resonances during rotor starting and the rotors must not be run continuously at the RPM that excites them [9].

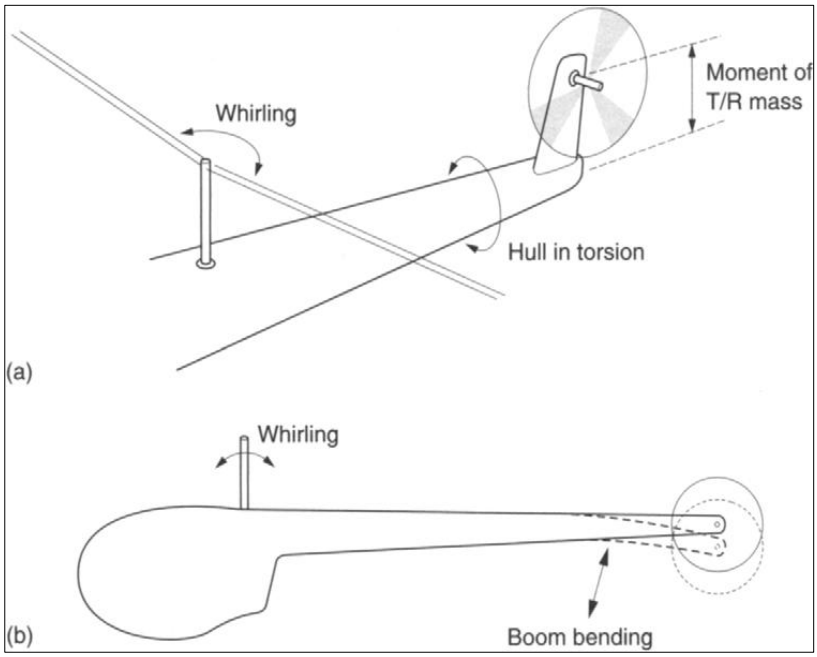

Figure 1. 2(a): Main rotor lateral rocking during start-up places in the tail boom under a torsional loading. The inertia of the tail rotor and gear box may combine with torsional stiffness of the tail boom to produced a resonance. (b) Force and aft-rocking causing bending loads in the tail boom with the potential for resonance [9].

As the tail boom is in the downwash of the main rotor, it will create aerodynamic forces. Figure 1.3(a) shows that in still air the force will be primarily downwards, possibly with a slight, and beneficial, sidethrust due to swirl. However, if there is a crosswind, the resultant of the crosswind and the downwash will be a non-vertical RAF seen by the boom. This may result in a significant amount of boom lift, shown at Figure 1.3(b) which is not necessarily in a useful direction. If the boom lift opposes the tail rotor thrust, this may restrict the crosswind hovering performance. A possible solution is the addition of a boom strake mounted high on the boom. This has the effect of causing early separation and a reduction in the amount of lift

developed. A cylindrical shape may be great for the pressurized hull of an airliner that goes the way it is pointing, but it is generally less than ideal for transverse flow. This is because transverse airflow across a cylindrical shape is unstable. Separation takes place from alternate sides causing lift in alternate directions. Those spiral strakes fitted to factory chimneys are designed to cause flow separation at defined points in order to prevent shaking in a wind. A rounded helicopter hull or boom will also suffer from an indeterminate separation point and this may result in chaotic shaking in the hover. In this case a strake fitted low on the boom will produce a defined separation point and reduce the shaking. Boom strakes generally align reasonably well with airflow in cruise and so have little detrimental effect [9].

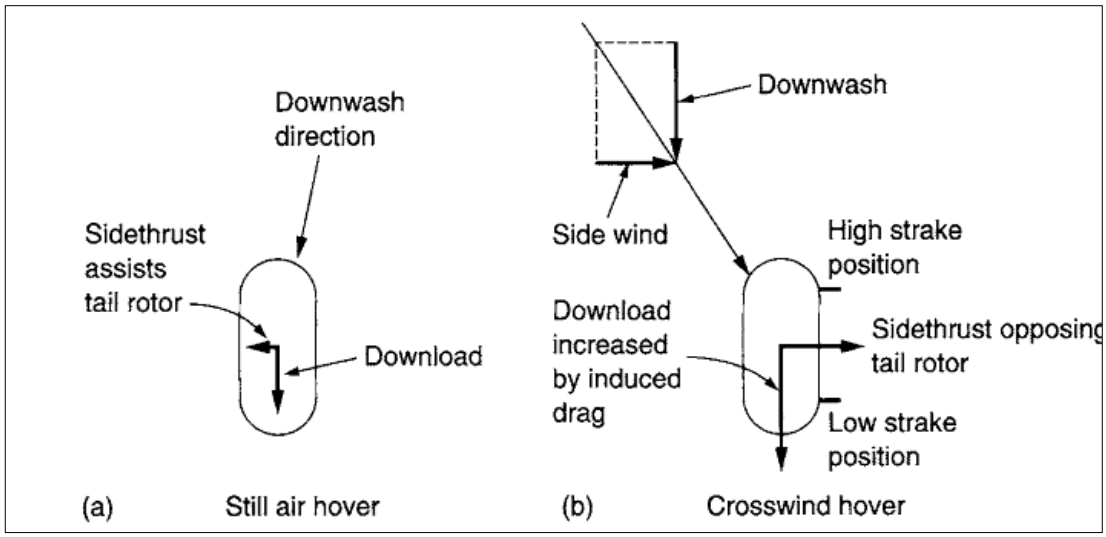

Figure 1.3(a) : In still air hover, downwash on the tail boom is vertical except for the swirl component.(b) In crosswind hover, the resultant airflow direction due to downwash and wind may cause significant boom lift. If this opposes the tail rotor thrust and crosswind hover performance may be impaired. A high-mounted boom strake may be uses to suppress boom lift in crosswinds, whereas a low-mounted boom strake may be used to define a separation point for downwash in the hover and thereby reduce shaking [9].

In 1995, AS-350 Squirrel helicopter tail boom was modeled by Aeronautical and Maritime Research Laboratory. Figure 1.4 shows that AS-350 Squirrel helicopter structure.

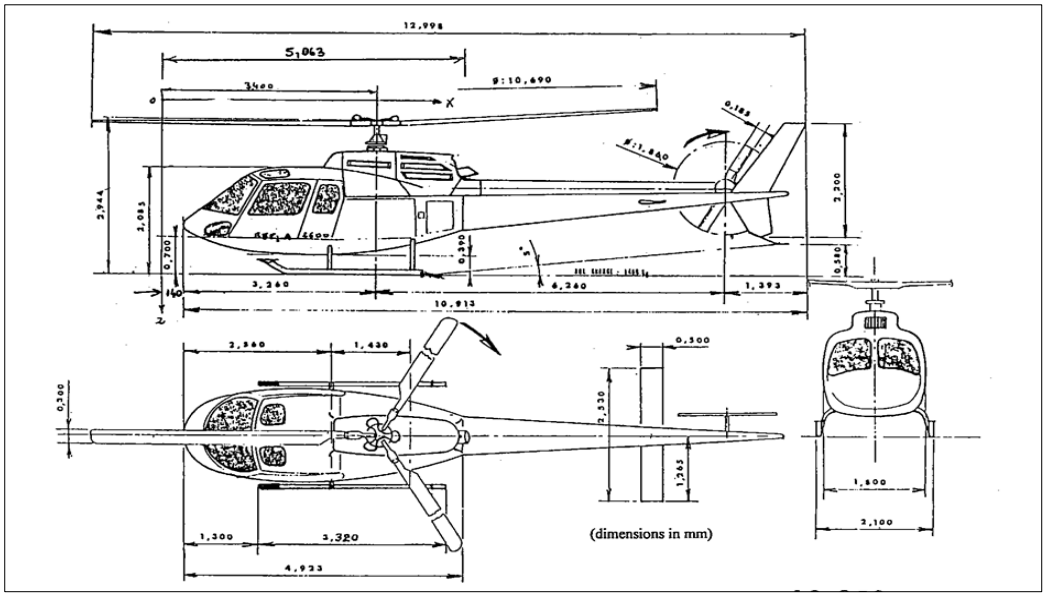

Figure 1.4: AS-350 Squirrel Helicopter [10].

Aluminum alloys 2024 tail boom was strength with stiffeners. The effect of various skin thickness combinations. The problem of AS-350 helicopter tail boom buckling had been indicated. Therefore, finite analysis conducted for static. The finite element model is show in Figure 1.5.

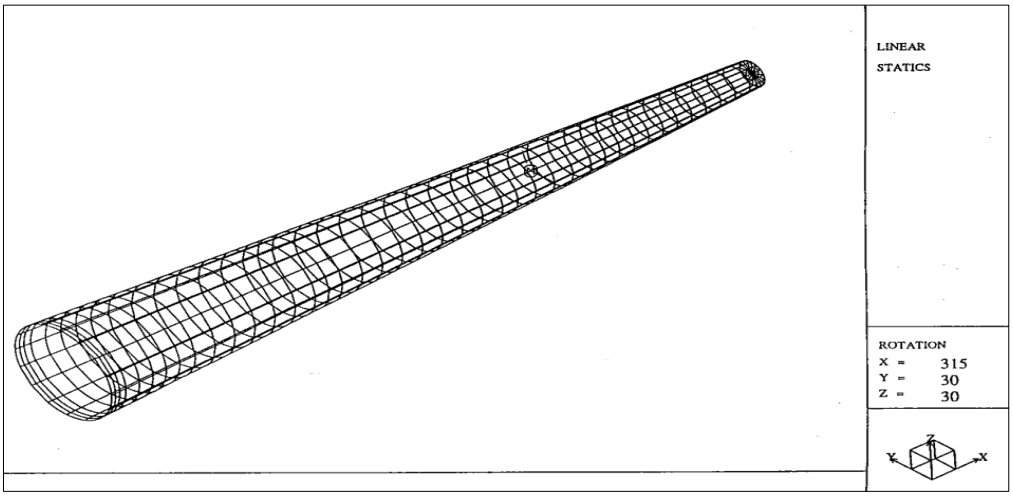

Figure 1.5: AS-350 helicopter finite element model [10].

In our country, the tail cones of A400M are produced in TUSAS. Figure 1.6 shows tail cone of A400M.

Figure 1.6: The tail cone of A400M [11].

1.3 Objectives

Helicopter manufacturers have long recognized the benefits of composites in critical aircraft components. In today's military rotorcraft, composites regularly constitute 50 to 80 percent of the airframe by weight. In this study, an unmanned helicopter tail cone is produced with polymer matrix composite.

Tail booms are the structures connecting the tail rotor to the fuselage. It is mainly subjected to the pitching moment and torsion. Because it is long to obtain the enough distance between the tail rotor and the main rotor, the materials used for manufacturing the tail boom needs to be a lightweight material. The goal of this thesis was written in order to examine the properties of the composite tail cones are used in helicopters. For this reason, hand- layup technique was used for two different composite tail cones. One is manufactured with honeycomb between 2-plies carbon fiber and other is manufactured with 3-plies carbon fiber and it is strengthened by composite stiffeners. Bending, torsional-bending features of two different composite tail cones are compared with each other. In test results, bending and torsion –bending features of the tail cone manufactured with honeycomb between two plies carbon fibers is better than the tail cone manufactured with three-ply carbon fiber and stiffeners. As a result, The tail cone that manufactured with honeycomb between two-plies carbon fibers is more suitable than the tail cone manufactured with three-plies carbon fiber and stiffeners. According to this test result, unmanned helicopter tail cone produced with honeycomb between 4-plies carbon fiber. Unmanned helicopter tail cone was produced with hand lay-up technique.

After that, unmanned helicopter tail boom structure was modeled by using ANSYS finite element software. Static analysis was achieved for bending and torsional bending load. Experimental and numerical results are compared with each other.

Also, cured features of epoxy is investigated with Differential Scanning Calorimetry.

2. COMPOSITE MATERIALS

A composite material is a material system consisting of two (or more) materials, which are distinct at a physical scale greater than about $1x10^{-6}$(1 μm) and which are bonded together at the atomic and/or molecular levels [12].

Composites have been routinely designed and manufactured for applications in which high performance and light weight are needed.

The growth in composite usage also came about because of increased awareness regarding product performance and increased competition in the global market for lightweight components. Among all materials, composite materials have the potential to replace widely used steel and aluminum, and many times with better performance [13].

2.1 History of Composite Materials

Composite materials are used throughout history of mankind. The earliest known composite material is mud brick. Mud brick is made of mixture of clay, mud, sand, and water mixed with a binding material such as rice husks or straw [14].

The history of modern composite materials began in 1937 [14]. Owens Corning Fiberglass Company initiated the selling of fiberglass to interested parties around the United States. A Japanese company (Nitto Boseki) also manufactured fiberglass and attempted to market the fibers in Japan and the United States. The fiberglass salesmen had long realized that the aircraft industry was, in particular, a likely customer for this new type of material because many small and vigorous aircraft companies seemed to be creating new aircraft designs and innovative concepts in manufacturing almost daily with many of these innovations requiring new materials. First, Douglas Aircraft bought the roll of fiberglass [14]. They had a bottleneck in the making of metal molds for their sheet metal forming process. Each altered aircraft

design needed new molds and metal molds were expensive and had long lead times. Douglas engineers tried using cast plastic molds and in collaboration with Owens Corning Fiberglass dies were made using the new fiberglass materials and phenolic resin. Reinforced plastic dies for prototype parts became the standard [14].

In 1961 a patent was issued to A. Shindo for experimentally producing the first carbon (graphite) fiber but Courtalds Limited of the United Kingdom was the first to produce commercially viable carbon fibers several years later [14].

New fibers were also introduced with boron filaments becoming available in 1965 and aramid fibers (Kevlar®) offered commercially by DuPont in 1971 [13]. Today continues work on composite materials and new composite material has been developed day by day.

2.2 Classification of Composite Materials

In general, composites are classified according to matrix, fiber and constituents.

2.2.1 Based on matrix material

According to matrix materials, composites are classified as metal, ceramic and polymer.

2.2.1.1 Ceramic matrix composite

Ceramic matrix composite materials consist of ceramic matrix and reinforced ceramic disperse phase. These phases may be oxide or non- oxide. Also, ceramic matrix composites are reinforced by either continuous or discontinuous fibers. Advantages of ceramic matrix composites include high strength, high service temperature limits for ceramics, hardness, chemical inertness, low density and, high toughness.

Ceramic matrix composites find increased applications in high-temperature areas in which metal and polymer matrix composites cannot be used [15].

The most common applications of ceramic matrix composite are utilized in the manufacturing of gas turbine.

2.2.1.2 Metal matrix composite

When the matrix is a metal or its alloys, this composite is metal matrix composites (MMC). In general, properties of metal matrix composites can be listed as light weight, good thermal conductivity, ductility. The performance of these materials, i.e. their characteristics in terms of physical and mechanical peculiarity, depend on the nature of two components (chemical composition, crystalline structure, and in the case of reinforcement, shape, and size), the volume fraction of the adopted reinforcement and production technology [16].

In general, MMCs are classified according to type of used reinforcement and their geometrical characteristics. Two basics categories exist:

- Continuous reinforcement composites
- Discontinuous reinforcement composites

One of the most widely used metal matrix composite materials is the reinforcements are inserted into the composite as aluminum metal matrix composites. Especially, aluminum metal matrix composites are preferred by aerospace industry. Aluminum matrix composites can be used as long fiber (boron, silicon carbide, alumina and graphite), short fiber (alumina, alumina-silicon), whiskers (silicon carbide), particle (silicon carbide, boron carbide) [16].

2.2.1.3 Polymer matrix composite

Polymer matrix composite materials consist of fibrous reinforcing dispersed phase (carbon, glass, aramid) in a polymer (resin) matrix. Thermoplastic and thermoset polymers can be used in composite materials. Thermosets are processed at lower temperatures than thermoplastics. Also, chemical resistance of thermosets is better than thermoplastics, but toughness values of thermosets are lower than thermoplastics [16].

Carbon, glass and aramid (Kevlar) fibers are used to reinforced in polymer matrix composites. Commercial grade carbon fibers have tensile strength values between 207 MPa and 1035 MPa. Carbon-fiber reinforced composite materials are used widely in aircraft industry [16].

The properties of polymer matrix composite materials are high-strength, dimensional- thermal stability, hardness, corrosion resistant.

2.2.2 Based on reinforcing materials

According to reinforcing materials, composites are classified as particular, fibrous and laminate.

2.2.2.1 Particulate composite

Particulate composites consist of a matrix reinforced by a dispersed phase in form of particles. Figure 2.1 shows a schematic drawing of particulate composites. Particulate composites have advantages such as improved strength, increasing operating temperature and oxidation resistance etc. For example, most polymers in homogenous form are glassy and brittle and the addition of rubber particles to a polymer matrix can greatly improve the impact resistance of the material [17].

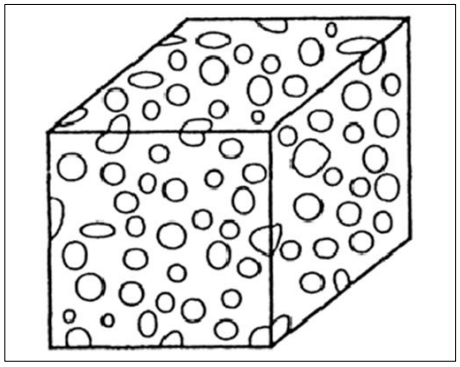

Figure 2.1: Particulate composite materials [17].

The particles may have any shape or size but generally spherical, ellipsoidal, polyhedral or irregular in shape. The particles can be either metallic or nonmetallic as can be matrix [17].

2.2.2.2 Fibrous composite

A fibrous composite is defined as a composite that consists of thin slivers of one material embedded in another material. Composite materials owe their remarkable characteristics to the fibers which are used to reinforce the matrix. Fibers can be divided into three groups as natural, regenerated and synthetic. Artificial fibers are only just over 100 years old and the earliest produced were based on the naturally

occurring cellulose molecule. The common fiber used for engineering applications is carbon, aramid (Kevlar), glass and their hybrid. Figure 2.2 shows a schematic figure of fibrous composites [17].

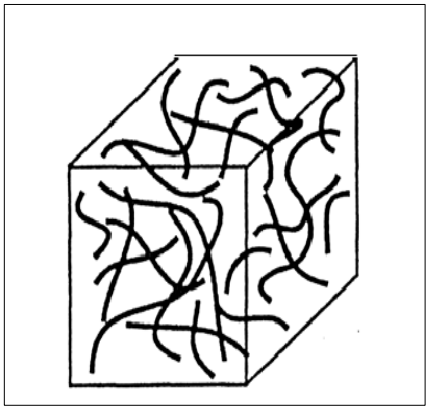

Figure 2.2: Fibrous composite materials [17].

The main functions of the fibers in a composite are [17]:

- To carry the load. In a structural composite, 70 to 90% of the load is carried by fibers.
- To provide stiffness, strength, thermal stability, and other structural properties in the composites.
- To provide electrical conductivity or insulation, depending on the type of fiber used.

2.2.2.3 Laminate composite

A laminate is a material that can be constructed by uniting two or more layers of material together. Figure 2.3 shows that laminate composite materials. The layers of laminated composite materials may be different single materials, such as clad metals that are bond together or the same materials, such as wood put together with different orientations. The layers may be composites themselves, such as fibrous composite layers placed, so that different layers have different characteristics. This type of composite is the most commonly encountered laminated composite materials used in design of high performance structures [18].

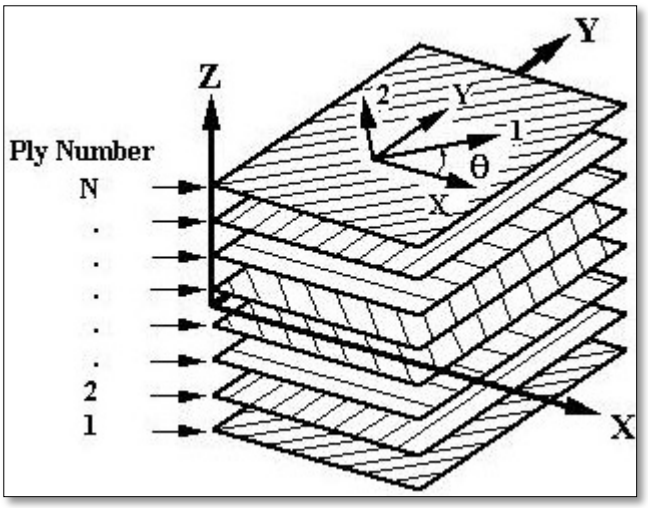

Figure 2.3: Laminate composite materials [19].

3. MANUFACTURING OF COMPOSITE COMPONENTS

3.1 Introduction

Composite materials comprise two or more materials. Therefore, processing of composite is the science of transforming materials from one shape to the other. There are various types of composites processing techniques available to process the various types of reinforcements and resin systems [13].

3.2 Manufacturing Methods

Several commonly used manufacturing methods are listed below and briefly described in Section 3.2.1 through Section 3.2.8:

- Hand (wet) lay-up/automated lay-up
- Pultrusion
- Filament winding
- Resin transfer molding (RTM)
- Sheet molding compound (SMC)
- Injection molding
- Compression molding
- Extrusion

3.2.1 Hand (wet) lay-up/automated lay-up

The hand (wet) lay-up and automated lay-up processes have been used to produce a significantly large number of fiber reinforced polymer composite products [20]. More than half of structural composites in the aerospace industry are made from hand layup processes [20]. In the hand lay-up process, fibers are impregnated with resin using a handheld roller and brushes. Each fiber/fabric layer is pressed with hand rollers to ensure proper and uniform wetting of the reinforcement. Some of the structural parts are sandwiched with honeycomb or rigid foam blocks as core

material. Hand lay-up processes can utilize resin pre-impregnated reinforcement called “prepreg” to provide consistent control over reinforcement to resin ratio by weight or volume. Several variations in the hand/automated lay-up manufacturing process are possible [20]. Figure 3.1 shows a schematic drawing of hand lay-up technique.

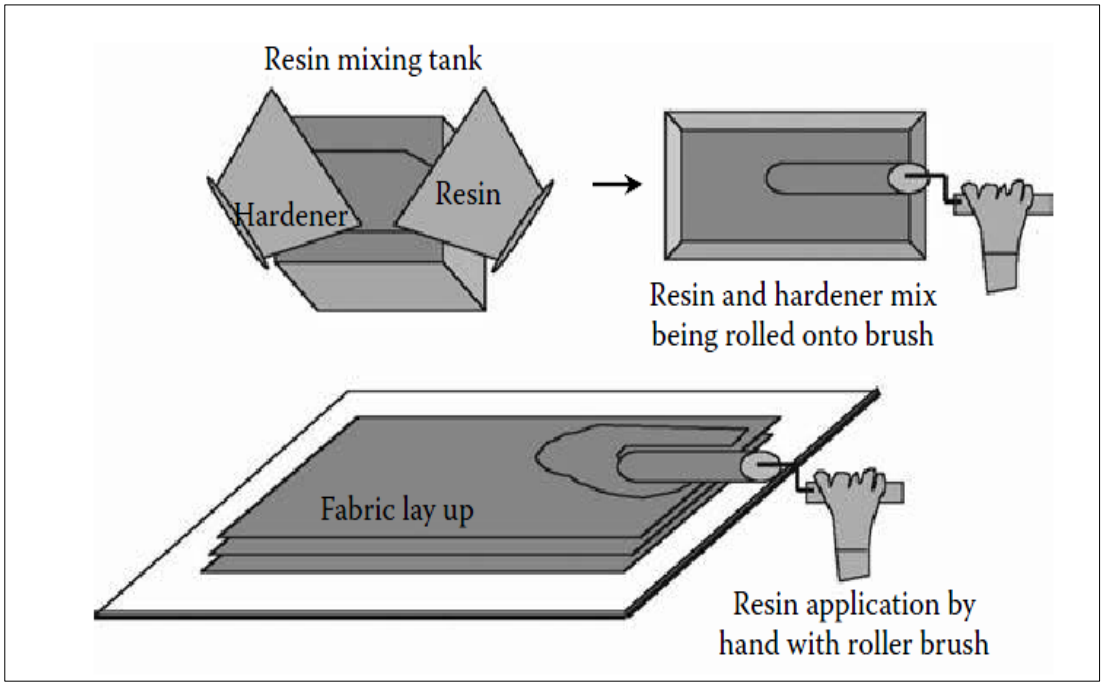

Figure 3.1: Schematic representation of a hand lay-up process [20].

In the automatic lay-up procedure, multiaxis Computer Numeric Control (CNC) machines are used to lay prepreg tape or prepreg fibers [20]. Prepreg curing is typically carried out with the use of ovens, heated-platen presses, or autoclaves. Room temperature curing can take as long as two hours, whereas heat-assisted curing can take about one half-hour or less. Curing can also be carried out with vacuum bag molding, wherein a nonadhering plastic film -usually polyester- is sealed around the mold plate and lay-up assembly [20]. A vacuum force is applied through the bag covering the whole fiber/fabric lay-up to draw out both excess resin and entrapped air. For vacuum bag and autoclave assisted curing lay-up processes, some of the accessories needed include separator films, bleeder plies, vent cloth, vacuum lines and fittings, edge seals, thermocouples, and autoclave units [20]

3.2.2 Pultrusion

The term pultrusion combines the words, "pull" and "extrusion". Extrusion is the pushing of material, such as a billet of aluminum, through a shaped die. Whereas pultrusion, is the pulling of material, such as fiberglass and resin, through a shaped die. The pultrusion process starts with racks or creels holding rolls of fiber mat or doffs of fiber roving [21]. Most often the reinforcement is fiberglass, but it can be carbon, aramid, or a mixture. This raw fiber is pulled off the racks and guided through a resin bath or resin impregnation system. Resin can also be injected directly into the die in some pultrusion systems. The raw resin is almost always a thermosetting resin, and is sometimes combined with fillers, catalysts, and pigments. The fiber reinforcement becomes fully impregnated (wetted-out) with the resin such that all the fiber filaments are thoroughly saturated with the resin mixture [21].

As the resin rich fiber exits the resin impregnation system, the un-cured composite material is guided through a series of tooling. This custom tooling helps arrange and organize the fiber into the correct shape, while excess resin is squeezed out, also known as “debulking.” This tooling is known as a “pre-former.” Often continuous strand mat and surface veils are added in this step to increase structure and surface finish [21].

Once the resin impregnated fiber is organized and removed of excess resin, the composite will pass through a heated steel die. Precisely machined and often chromed, the die is heated to a constant temperature, and may have several zones of temperature through-out its length, which will cure the thermosetting resin. The profile that exits the die is now a cured pultruded Fiber Reinforced Polymer (FRP) composite [21].

This FRP profile is pinched and pulled by a “gripper” system. Either caterpillar tracks or hydraulic clamps are used to pull the composite through the pultrusion die on a continuous basis. At the end of this pultrusion machine is a cut-off saw. The pultruded profiles are cut to the specific length and stacked for delivery

3.2.3 Filament winding

Filament winding is a process in which resin-impregnated fibers are wound over a rotating mandrel at the desired angle [22]. A typical filament winding process is shown in Figure 3.2, in which a carriage unit moves back and forth and the mandrel rotates at a specified speed. By controlling the motion of the carriage unit and the mandrel, the desired fiber angle is generated [22]. The process is very suitable for making tubular parts. The process can be automated for making high-volume parts in a cost-effective manner. Filament winding is the only manufacturing technique suitable for making certain specialized structures, such as pressure vessels [22].

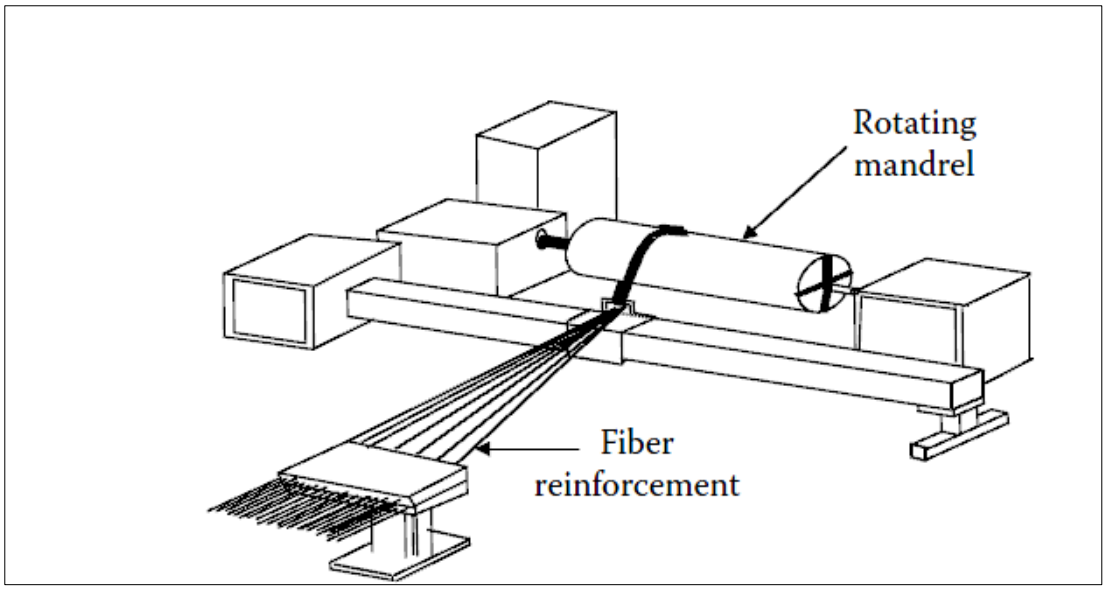

Figure 3.2: Schematic of a filament winding process [22].

3.2.4 Resin transfer molding (RTM)

Resin transfer molding is also known as a liquid transfer process. Resin transfer molding is a class of manufacturing processes used to produce polymer composite components and structures [20]. In RTM process, a fibrous preform material is placed into to the mold. A matching mold half is mated to the first half and the two are clamped together and sealed to prevent leakage before a liquid resin is injected. Using dispensing equipment, a pressurized mixture of thermoset resin, a catalyst, color, filler, etc., is pumped into the mold using single or multiple ports in the mold. After curing for 6 to 30 min, depending on the cure kinetics of the mixture, the part is

then removed from the mold. Thus, RTM results in the production of structural parts with good surface finish on both sides of the part [20].

The main issues in the RTM process are resin flow, curing and, heat transfer in porous media. The process involves injecting a precatalyzed thermosetting resin under pressure into a heated mold cavity that contains a porous fiber preform. During mold filling, the resin flows into the mold and experiences exothermic curing reactions, causing its viscosity to increase over time and finally solidification. After the fiber preform is completely saturated with resin, cure reactions continue past the gel-point to form a cross-linked polymer [20].

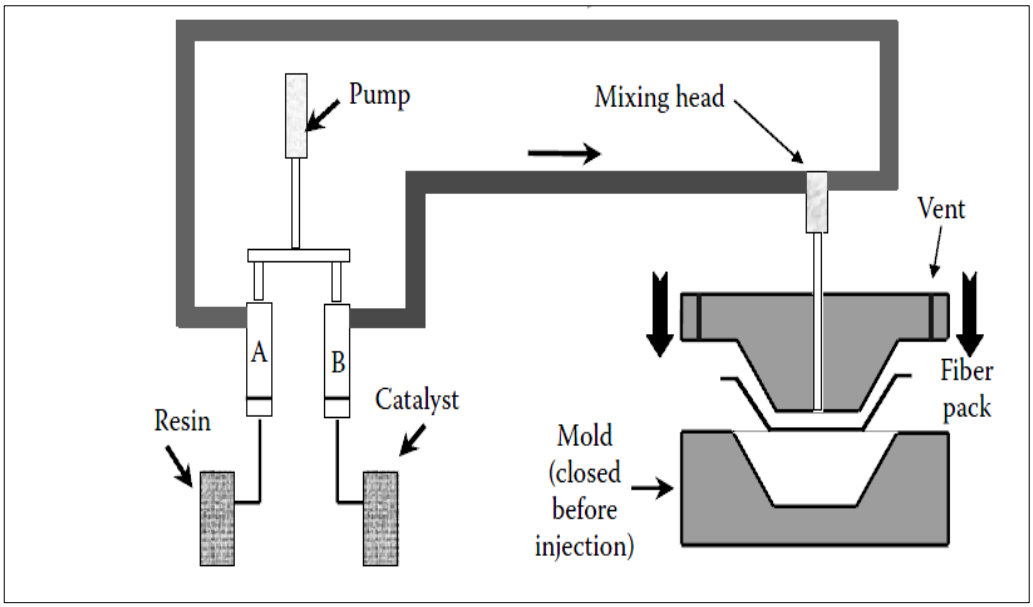

Figure 3.3: Resin transfer molding process [20].

The steps during the RTM process are summarized below:

- A thermoset resin and catalyst are placed in tanks A and B of the dispensing equipment.
- A release agent is applied to the mold for easy removal of the part. Sometimes, a gel coat is applied for good surface finish.
- The preform is placed inside the mold and the mold is clamped.
- The mold is heated to a specified temperature.
- Mixed resin is injected through inlet ports at selected temperature and pressure. Sometimes, a vacuum is created inside the mold to assist in resin flow as well as to remove air bubbles.

- Resin is injected until the mold is completely filled. The vacuum is turned off and the outlet port is closed. The pressure inside the mold is increased to ensure that the remaining porosity is collapsed.
- After curing for a certain time (6 to 20 min, depending on resin chemistry), the composite part is removed from the mold.

Recently, resin transfer molding has gained importance in the composite industry because of its potential to make small to large complex structures in a cost- effective manner. Figure 3.3 shows a schematic drawing of resin transfer molding. RTM is used in automotive, aerospace, sporting goods, and consumer product applications [20].

3.2.5 Sheet molding compound

Sheet molding compound process is the most important process technology for fiber reinforced polymers [20]. It primarily consists of polyester and vinyl ester resins, chopped glass fibers, inorganic fillers, additives, and other materials. The SMC material (sheet) is cut to the necessary dimensions and stacked or oriented in the mold as per the design configuration [20]. Curing is achieved through a heated die under pressure. The process temperature varies from 120-175^{o}C, whereas the molding pressure ranges from 250 to 3000 psi. The time for each molding cycle can vary from 1 to 4 min and depends upon the part thickness, mold temperature, fiber and resin quantity, and the amount of catalyst. After removing the molded part, it may be subjected to secondary operations such as stud insertion, piercing, bonding, deflating, and others. SMC consists of any one of the following fiber types:

- Random chopped fibers
- Continuous unidirectional fibers
- Combined random chopped fibers
- Discontinuous unidirectional fibers of approximately 4 in length [20].

Figure 3.4 shows a sketch of the sheet molding compound process.

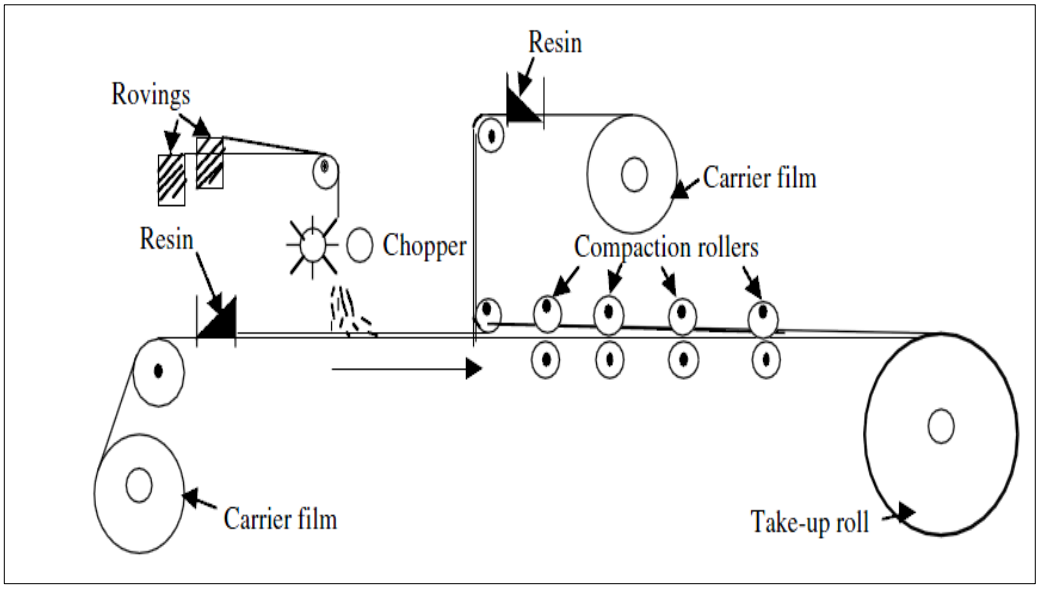

Figure 3. 4: Sheet molding compound process [20].

3.2.6 Injection molding

The injection molding process is mainly used for making parts from thermoplastic polymers [22]. Injection molding is an economical and very efficient method of producing injection molded parts. It can produce millions of parts with exactly the same shape, dimension, and quality. Some examples of injection molded parts are the mobile phones, mouse, keyboard, and many components found inside the automobile [22].

It is possible to inject short fibers mixed in an uncured resin into molds in much the same way as many unreinforced plastics are molded. Compounds with fiber lengths up to 30 mm are used and are fed manually or automatically from a roll or bulk form of the material. The steel molds are heated in the temperature range 140–160 °C. The technique is suitable for making small thick specimens and it is possible to produce up to 60 per hour [22].

3.2.7 Compression molding

Compression molding is very popular in the automotive industry because of its high volume capabilities. Compression is a process in which a molding polymer is squeezed into a preheated mold taking a shape of the mold cavity and performing curing due to heat and pressure applied to the material [22]. Figure 3.5 shows a sketch of the compression molding process.

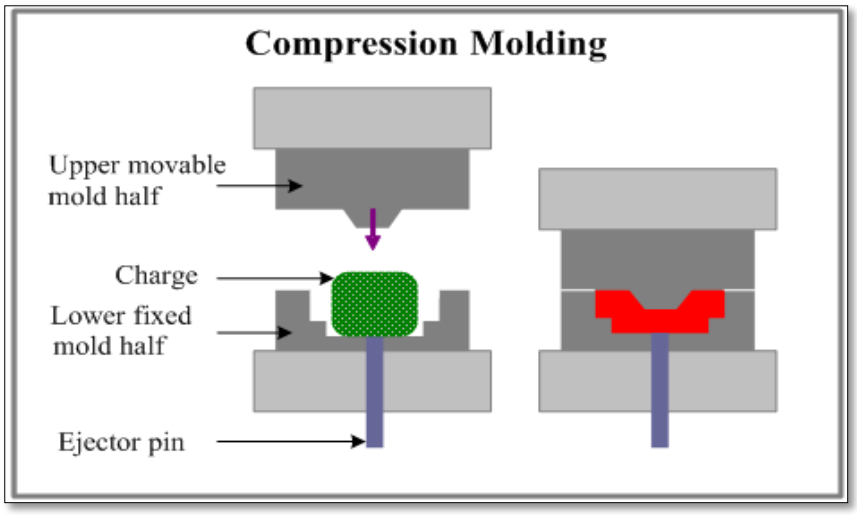

Figure 3.5: Compression molding process [23].

3.2.8 Extrusion

Extrusion process is used for making continuous parts with thermoplastic polymers. In this process, thermoplastic polymer in the form of pellets and flakes is placed in the vertical hopper of the extrusion machine that feeds into a long horizontal chamber — typically consisting of four or more heating zones from start to exit — with continuously revolving screws [22]. Screw movement forces the softened resin out of the heating chamber through a die. Hot polymer extruded from the die is fed onto a conveyor belt and quenched (cooled) through water immersion or air-blowing techniques. The die is formed in the shape of the final product, e.g., tubes, rods, continuous films, and shapes. Biaxial polymer geogrids used for soil strengthening are manufactured from extrusion process with the use of high-density polyethylene or polypropylene [22].

4. HELICOPTER COMPOSITE TAIL BOOM STRUCTURE AND CHACTERIZATION

4.1 Introduction

The tail boom effectively couple two masses together; the main rotor and the tail rotor. The main rotor of a helicopter simply spins the fuselage in the opposite direction without a tail rotor. In twin-rotor helicopters, the torque produced by the rotation of the front rotor is offset by the torque produced by a counter rotating rear rotor. Because it is long to obtain the enough distance between the tail rotor and the main rotor, the materials used for manufacturing the tail boom needs to be a lightweight material. It is mainly subjected to the pitching moment and torsion. Therefore, an unmanned aerial vehicle tail boom is produced with wet hand lay-up technique. The vacuum is applied during the production at elevated temperature. The tail cone is tested under bending and a combined loading including bending and torsion. Furthermore, tail cones with different orientation have been created by using ANSYS software, and they have been compared with each other.

4.2 Materials Tests

4.2.1 Differential scanning calorimetry

Differential Scanning Calorimetry (DSC) measures the temperatures and heat flows related to transition in materials as a function of time and temperature in a controlled atmosphere. DSC tests provide quantitative and qualitative information about physical and chemical changes that include endothermic or exothermic process, or changes in heat capacity through the measurement of absorption or release of energy. In a DSC experiment the difference in energy input to a sample and a reference material is measured while the sample and reference are subjected to a controlled temperature program as shown in Figure 4.1. DSC requires two pans equipped with

thermocouples in addition to a programmable furnace, recorder, and gas controller. The case of polymer or polymer composite materials, glass transition temperature (T_g) is very useful aspect which can be obtained from DSC. If output DSC data shifts upward suddenly at a certain temperature, this means more heat flow is needed to balance the temperature. This shows an increase in the heat capacity of sample. Namely, this happens because the polymer has just gone through the glass transition. Polymers have a higher heat capacity above the glass transition temperature than they do below it [24].

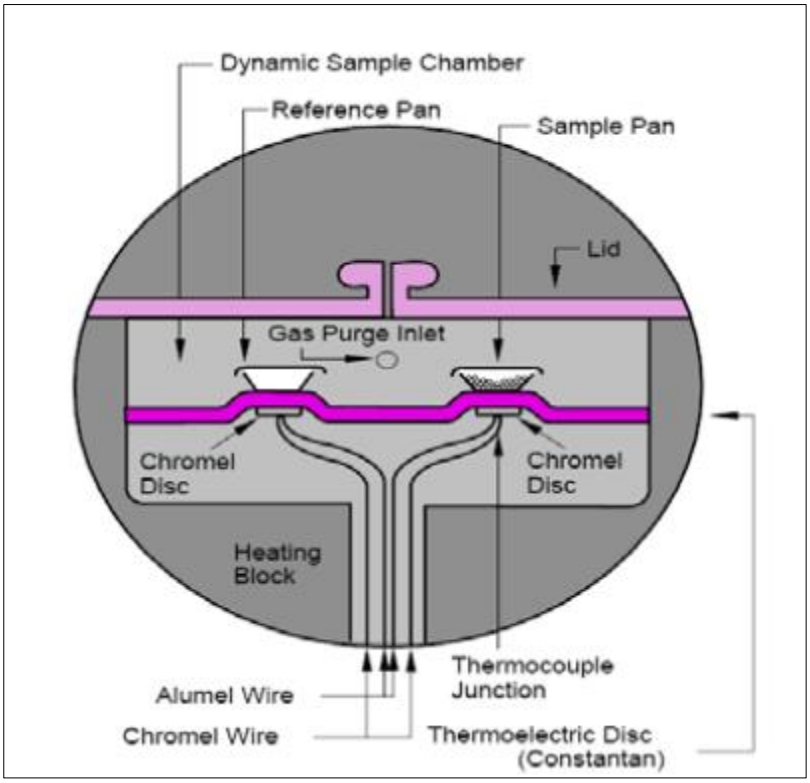

Figure 4. 1: Schematic differential scanning calorimetry [24].

The following features can be determined by DSC method.

- Glass transitions
- Melting and boiling points
- Crystallization time and temperature
- Percent crystallinity
- Heats of fusion and reactions

- Specific heat capacity
- Oxidative/thermal stability
- Rate and degree of cure
- Reaction kinetics
- Purity

A thermosetting resin undergoes an irreversible chemical reaction during curing. As the components in the resin system cure, heat is evolved by the resin, which is monitored by the DSC instrument. Figure 4.2 represent the changes taking place of cure is the temperature at which the heat flow deviates from a linear response and the exothermic peak temperature reflects the maximum rate of curing of the resin. At the completion of curing or crosslinking, the DSC heat flow returns to a quasilinear response. The area under the exothermic can be integrated to give the heat of cure, ΔHcure (J/g). As a thermosetting resin cures or crosslink, two main things happen [25]:

- T_g increases
- Heat of cure decreases

The changes in T_g and the heat of cure can be used to characterize and quantify the degree of cure of the resin system. As the resin system approaches complete cure, the T_g will achieve a maximum value, T_g [25].

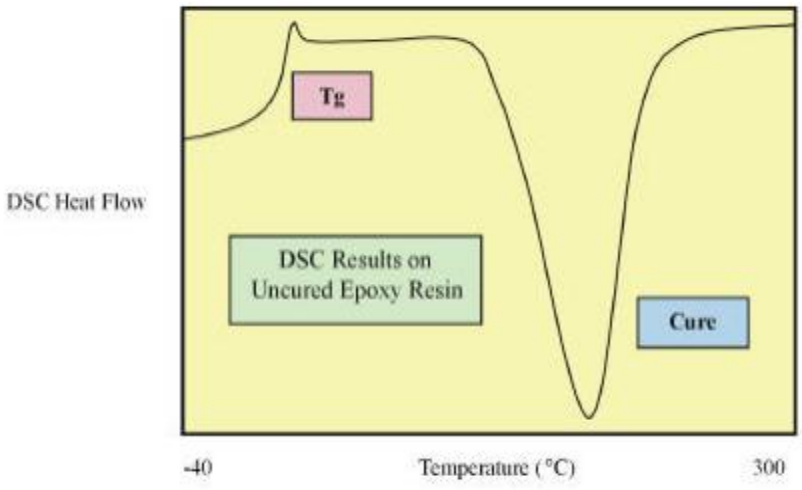

Figure 4.2: Increase in DSC Tg as a function of the cure for thermosetting resin [25].

The increase in the T_g observed as a function of curing represents the increase in the molecular weight of the resin system. The actual value of T_g is dependent upon the chemical make-up of the particular resin system. As the resin becomes more cross linked, the heat of curing becomes increasingly smaller and, as the material becomes completely [25].

According to DSC analysis in İTÜ Polymer Laboratory, the glass transition event, T_g, is observed at 0 °C as an exothermic stepwise increase. The endothermic peak temperature reflects the maximum rate of curing of the resin. The endothermic peak temperature is 58.45° C as shown in Figure 4.3.

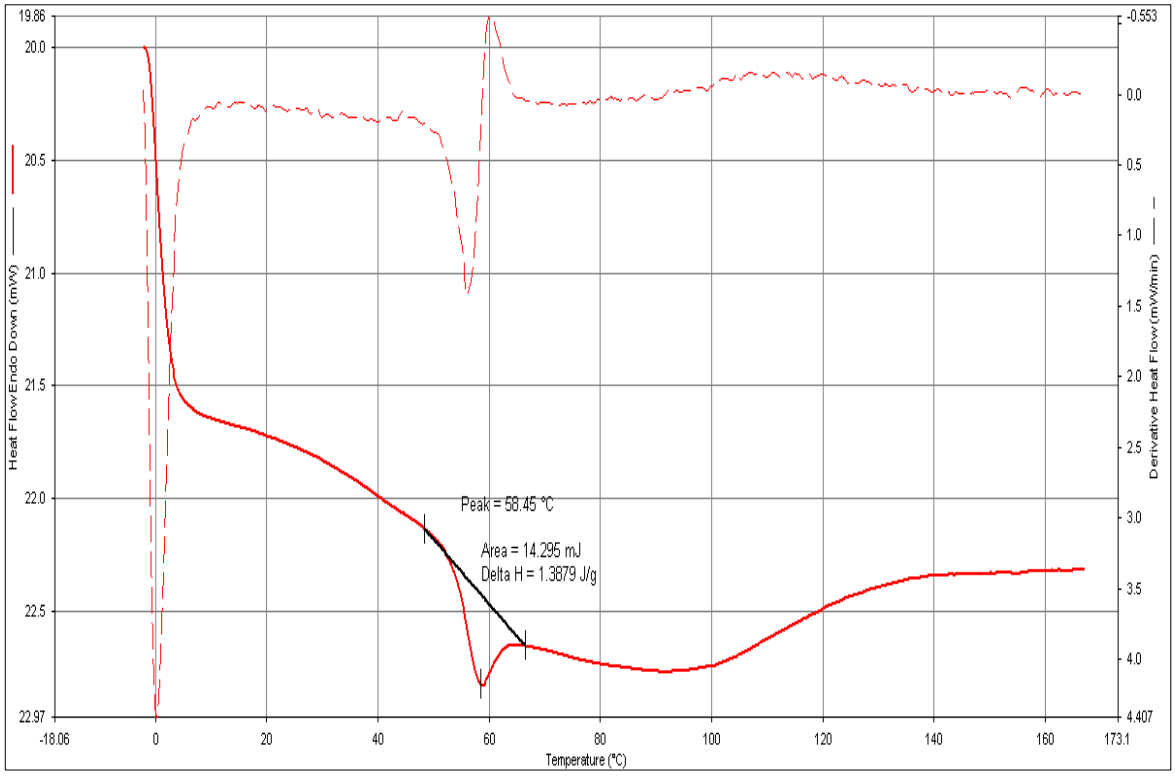

Figure 4.3: DSC analysis in İTÜ Polymer Laboratory.

According to the result of carbon fiber composite materials DSC analysis, optimum curing temperature is approximate 60º C. Therefore, the original composite tail cone was produced at 60º C.

4.2.2 X-ray diffraction

X-ray powder diffraction (XRD) is a rapid analytical technique primarily used for phase identification of a crystalline material and can provide information on unit cell dimensions. The analyzed material is finely ground, homogenized, and average bulk composition is determined.

Fundamental Principles of X-ray Powder Diffraction (XRD)

Max von Laue, in 1912, discovered that crystalline substances act as three-dimensional diffraction gratings for X-ray wavelengths similar to the spacing of planes in a crystal lattice. X-ray diffraction is now a common technique for the study of crystal structures and atomic spacing [24].

X-ray diffraction is based on constructive interference of monochromatic X-rays and a crystalline sample. These X-rays are generated by a cathode ray tube, filtered to

produce monochromatic radiation, collimated to concentrate, and directed toward the sample. The interaction of the incident rays with the sample produces constructive interference when conditions satisfy Bragg's Law ($n\lambda=2d \sin\theta$). This law relates the wavelength of electromagnetic radiation to the diffraction angle and the lattice spacing in a crystalline sample. These diffracted X-rays are then detected, processed and counted. By scanning the sample through a range of 2θ angles, all possible diffraction directions of the lattice should be attained due to the random orientation of the powdered material. Conversion of the diffraction peaks to d-spacings allows identification of the mineral because each mineral has a set of unique d-spacings. Typically, this is achieved by comparison of d-spacings with standard reference patterns [24].

All diffraction methods are based on generation of X-rays in an X-ray tube. These X-rays are directed at the sample, and the diffracted rays are collected. A key component of all diffraction is the angle between the incident and diffracted rays. Powder and single crystal diffraction vary in instrumentation beyond this [24].

X-ray diffractometers consist of three basic elements: an X-ray tube, a sample holder, and an X-ray detector. X-rays are generated in a cathode ray tube by heating a filament to produce electrons, accelerating the electrons toward a target by applying a voltage, and bombarding the target material with electrons. When electrons have sufficient energy to dislodge inner shell electrons of the target material, characteristic X-ray spectra are produced. These spectra consist of several components, the most common being K_α and K_β. K_α consists, in part, of $K_{\alpha1}$ and $K_{\alpha2}$. $K_{\alpha1}$ has a slightly shorter wavelength and twice the intensity as $K_{\alpha2}$. The specific wavelengths are characteristic of the target material (Cu, Fe, Mo, Cr). Filtering, by foils or crystal monochrometers, is required to produce monochromatic X-rays needed for diffraction. $K_{\alpha1}$and $K_{\alpha2}$ are sufficiently close in wavelength such that a weighted average of the two is used. Copper is the most common target material for single-crystal diffraction, with CuK_α radiation = 1.5418Å. These X-rays are collimated and directed onto the sample. As the sample and detector are rotated, the intensity of the reflected X-rays is recorded. When the geometry of the incident X-rays impinging the sample satisfies the Bragg Equation, constructive interference

occurs and a peak in intensity occurs. A detector records and processes this X-ray signal and converts the signal to a count rate which is then output to a device such as a printer or computer monitor [24]. Figure 4.4 shows an application of X-ray diffraction pattern.

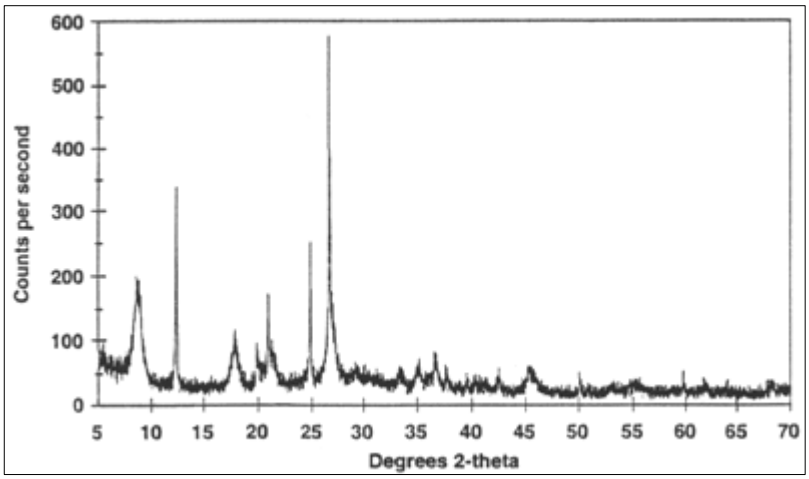

Figure 4.4: An application of X-ray diffraction pattern [26].

The geometry of an X-ray diffractometer is such that the sample rotates in the path of the collimated X-ray beam at an angle θ while the X-ray detector is mounted on an arm to collect the diffracted X-rays and rotates at an angle of 2θ. The instrument used to maintain the angle and rotate the sample is termed a goniometer. For typical powder patterns, data is collected at 2θfrom ~5° to 70°, angles that are present in the X-ray scan [25].

The properties of carbon fibers strongly depend on the structure. The properties include tensile modulus, tensile strength, electrical resistivity, and thermal conductivity. The structural aspects that are particularly important are the degree of crystallinity, the interlayer spacing (doo2), the crystallite sizes or, more accurately, the coherent lengths perpendicular (L,) and parallel (La) to the carbon layers, the texture (preferred orientation of the carbon layers) parallel and perpendicular to the fiber axis, the transverse and longitudinal radii of curvature (r, and r,) of the carbon layers, the domain structure, and the volume fraction, shape and orientation of microvoids [25].

Carbon fibres are produced from the polymere PAN. The atomic structure of carbon fiber is similar to that of graphite, consisting of sheets of carbon atoms (graphene

sheets) arranged in a regular hexagonal pattern. According to the studying Japan, carbon fiber composite was analyzed with XRD and x-ray diffraction peak was found as Figure 4.5. 2θ is approximately 26º

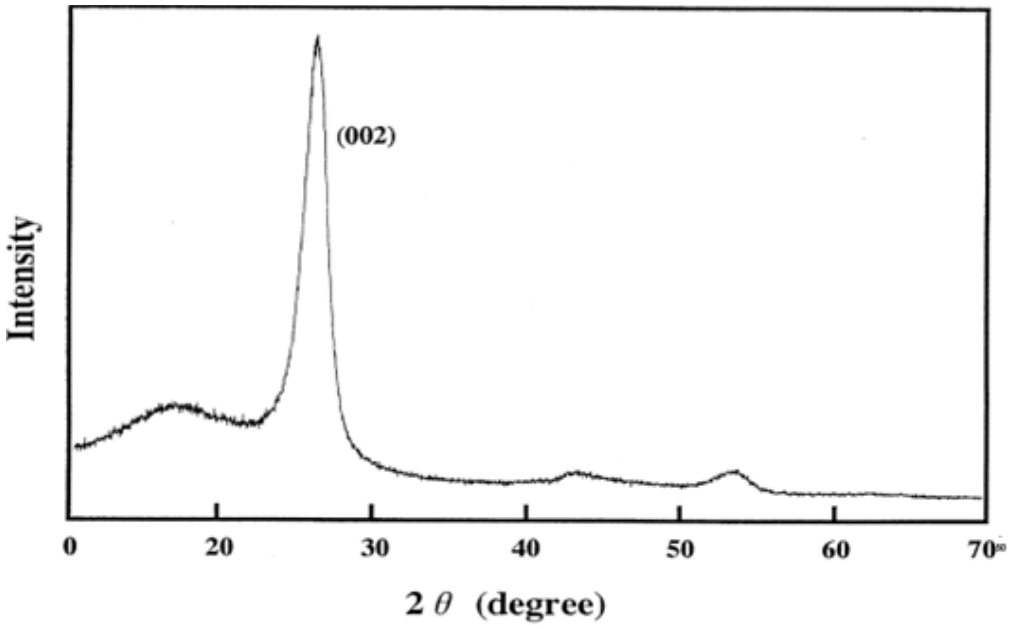

Figure 4.5: An example of carbon fiber x-ray pattern [27].

Carbon fiber composite material was analyzed with Bruker D8 Advance X-ray diffractometer in İTÜ. X-ray diffraction pattern of carbon fiber composite is shown in Figure 4.6. According to İTÜ PML Laboratory XRD diffraction study is similar to Figure 4.5. Carbon fiber composite diffraction degree is approximately 26º.

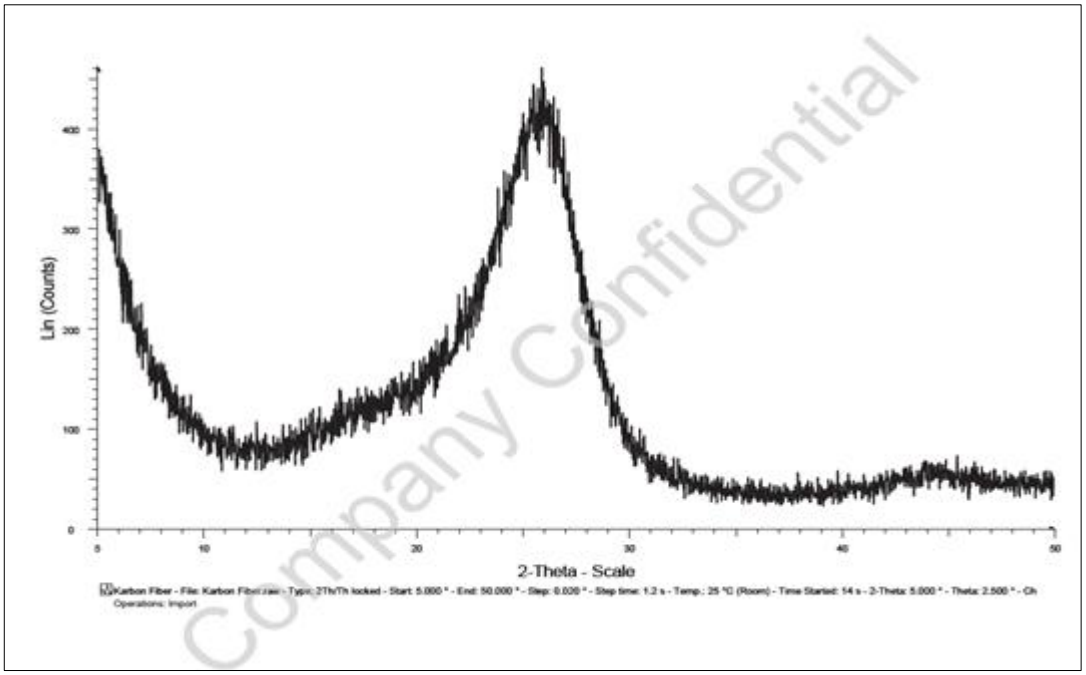

Figure 4.6: Carbon fiber composite X-ray pattern in Powder Metallurgy Laboratory in İTÜ.

4.3 The Production of Model Composite Tail Boom

Optimum weight and bending and torsional-bending properties were investigated for models of tail cone structure. Thus, optimization can be performed by maximization of the load for the specific weight, or by minimization of the weight of the structure the constraint of applied load. After that, optimum features were investigated and then original composite tail cone was produced in same conditions.

In this study, semi- conical shell was used to produce the tail cone. Generally, helicopter tail cone is greater than 1 meter. Model about half meter was used in this study. Firstly, wooden model was soaked and stretch film was covered on the model. Sufficient quantities of carbon fiber were cut and epoxy/hardener mixture was applied on carbon fibers. Two -plies carbon fibers were used in this process. Composite produced was put into Heatcon Composite System Machine. Heating was set to 60 $^{\circ}$C and pressure is set to 750 mb. Composite component was kept into machine about 10 hours.

To increase the resistance of the shell to buckling, it was strengthened by stiffeners, thus the critical load can be several times with only little addition of materials. Each

stiffener consisted of four layers of carbon fiber. Then, produced semi- conical shells combined with enough amount of epoxy/hardener mixture. In this wise, composite conical shells were produced. The other conical shell was produced with honeycomb between two layers of carbon fiber. Stiffeners were not used for this conical shell. Two different tail cones are shown in Figure 4.7.

Figure 4.7: Different conical shells.

After, different conical shells were modeled with ANSYS software program. Figure 4.8 shows an ANSYS model of conical shell.

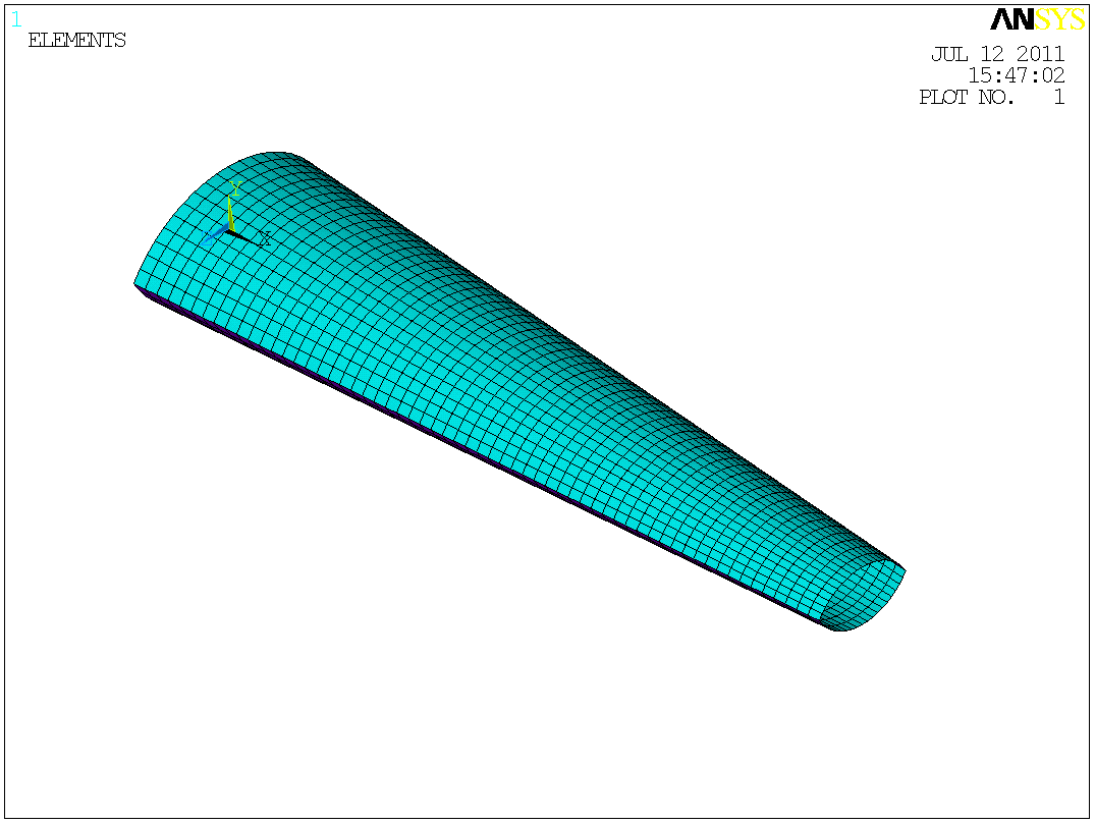

Figure 4.8: Finite element model of conical shell.

4.4 The Production of an Unmanned Aerial Vehicle Tail Boom

Previous experimental results showed that manufacture with honeycomb between two plies carbon fiber was more available for composite helicopter tail cone. Therefore, original composite tail cone was produced with honeycomb and carbon fibers.

This process was performed on 3 stages.

- Production with hand lay-up technique.
- Cutting each semi-conical structure and grinding.
- Horizontally strengthened with carbon tape band.

4.4.1 Production with hand lay-up technique

Totally, four plies carbon fiber and carbon fiber was used for unmanned helicopter tail cone. Cut four plies carbon fiber was weighed. In this process, the woven carbon (280 grams per square meter) was used in this production. Also, 2mm honeycomb

was used for this process. 700 grams epoxy/hardener mixture was prepared for 700 grams composite materials. 500 g epoxy was mixed with 200 g hardener. Firstly, wax is applied on mold lest carbon fiber does not adhere to the mold. Then, two plies carbon fiber was applied with sufficient quantity of epoxy/hardener mixture. After that, honeycomb was placed on the carbon fibers and then two plies carbon fiber was applied on the mold. Hand lay-up technique is shown in Figure 4.9.

Figure 4.9: Hand lay-up technique.

It should be sure that all composite materials were wet. Later, mold was placed on prepared vacuum bag. Pressure is set to 750 mb and mold is waiting about 24 hour at the room temperature. Blanket was used to a better power vacuum. Vacuum bag is shown in Figure 4.10.

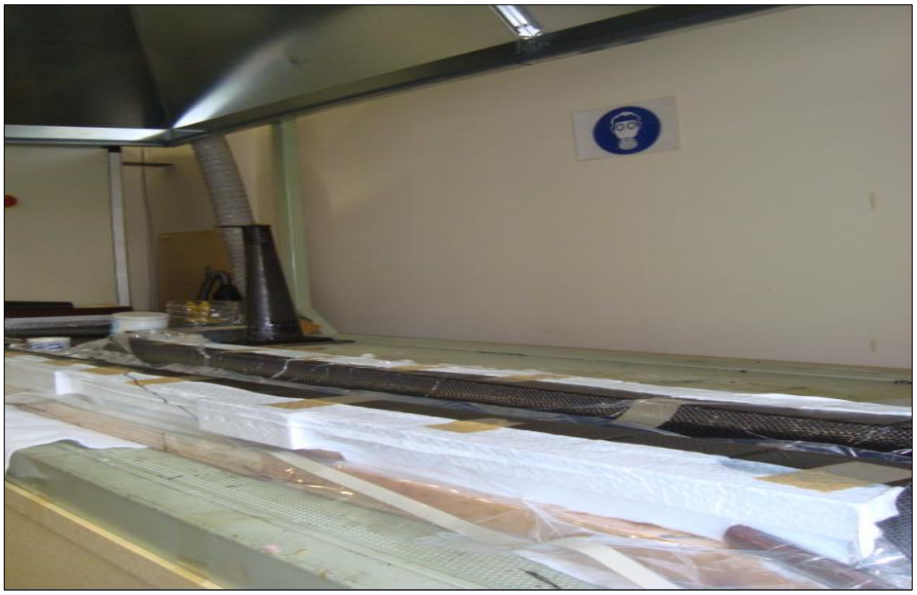

Figure 4.10: Vacuum bag.

4.4.2 Cutting each semi-conical structure and grinding

Two semi-conical shells were removed from vacuum bag. Semi-conical shells were properly cut with a grinding machine. Two semi-conical shells are shown in Figure 4.11.

Figure 4.11: Two semi-conical shells.

4.4.3 Horizontally strengthen with carbon tape band

Firstly, carbon fiber composite tail cone was sand-up to 5 cm. So, it provided that tape band show better adhesion feature. Horizontally, tape band was applied on sanded area. After that, composite tail cone was placed on vacuum bag. But, this vacuum bag made vacuum both inside and outside. Therefore, the vacuum bag was prepared both inside and outside. This section was the most difficult part of this process. Figure 4.12 shows sanded area.

Figure 4.12: Sanded area.

Two-ply carbon fiber tape band was applied with sufficient quantity of epoxy/hardener mixture both inside and outside on tail cone. Tail cone was placed on two vacuum bags. Pressure was set to 750 mb. At this stage, temperature was not applied on tail cone. Figure 4.13 shows that vacuum bags.

Figure 4. 13: Second vacuum bags.

After that, two plies carbon fiber tape band was pulled from outside and tail cone were placed on the vacuum bag. Figure 4.14 shows inside tape band after cured. Figure 4.15 shows outside tape band after cured.

Figure 4.14: Inside the tape band after cured.

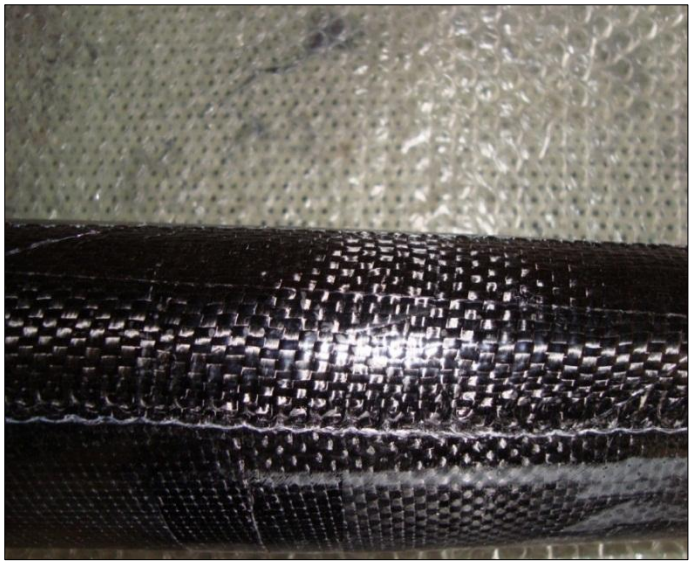

Figure 4. 15: Outside tape band after cured.

4.5 The Finite Element Model of an Unmanned Aerial Vehicle Tail Cone

A helicopter tail boom must be resistant to bending and torsional bending due to the aerodynamic effects. Therefore, the tail boom was modeled by using the ANSYS finite element software. Conical shell was modeled with 5 layers. Five layers contained 4-plies carbon fiber and honeycomb for conical shell. Six layers consist of 4-plies carbon fiber, honeycomb and in addition steel for text fixture.

4.5.1 CAD model

In this study, an unmanned aerial vehicle CAD model was designed by using CATIA software. Figure 4.16 shows dimensions of an unmanned aerial vehicle tail cone.

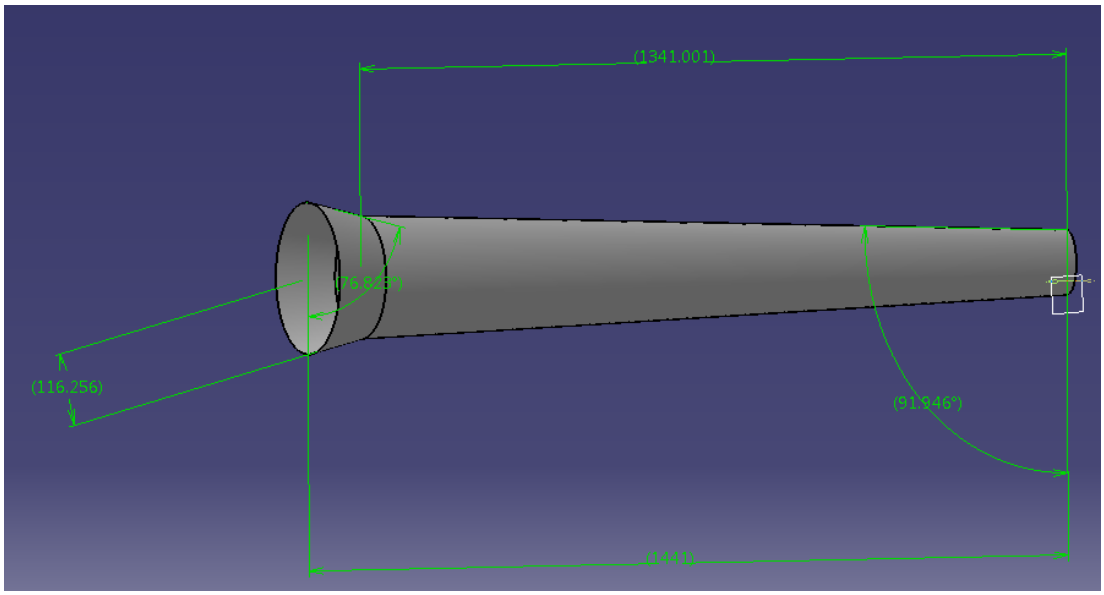

Figure 4.16: The dimensions of an unmanned aerial vehicle tail cone.

4.5.2 Select element type

Shell element is typically used for structure where the thickness is negligible compared to its length and width. The tail cone and test fixture were modeled by using the ANSYS finite element software. SHELL281 is suitable for analyzing thin to moderately-thick shell structures. It is an 8-node element with six degrees of freedom at each node: translations in the x, y, and z axes, and rotations about the x, y, and z-axes.SHELL281 may be used for layered applications for modeling laminated composite shells or sandwich construction [28].

Furthermore, BEAM4 was used for modeling torsional bending fixture. BEAM4 is a uniaxial element with tension, compression, torsion, and bending capabilities. The element has six degrees of freedom at each node: translations in the nodal x, y, and z directions and rotations about the nodal x, y, and z axes [28].

4.5.3 Define material property

The materials which were used for production of helicopter tail cone was defined. Honeycomb and bidirectional carbon fiber are orthotropic materials. Therefore, elasticity modulus, Poisson's ratio and shear modulus were defined for each composite materials. Table 4.1. shows mechanical properties of composite materials. Additionally, steel was defined for torsional bending test fixture.

Table 4. 1: Mechanical properties of composite materials.

Properties	Bidirectional Carbon Fiber	Honeycomb
E_x(MPa)	70000	50
E_y(MPa)	70000	50
E_z(MPa)	3000	50
ν_{xy}	0.3	0.2
ν_{yz}	0.4	0.2
ν_{xz}	0.4	0.2
G_{xy}(MPa)	10000	20
G_{yz}(MPa)	1000	20
G_{xz}(MPa)	1000	20

Three different sections were defined for tail cone and text fixture. Section ID1, ID2 and ID3 shows Table 4.2.

Table 4. 2: Section ID.

ID1		
Thickness (mm)	Material ID	Material
0.4	1	Carbon fiber
0.4	1	Carbon fiber
2	2	Honeycomb
0.4	1	Carbon fiber
0.4	1	Carbon fiber
ID2		
1.6	3	Steel
ID3		
0.4	1	Carbon fiber
0.4	1	Carbon fiber
2	2	Honeycomb
0.4	1	Carbon fiber
0.4	1	Carbon fiber
1.6	3	Steel

Figure 4.17 shows that the layers of the conical shell and text fixture.

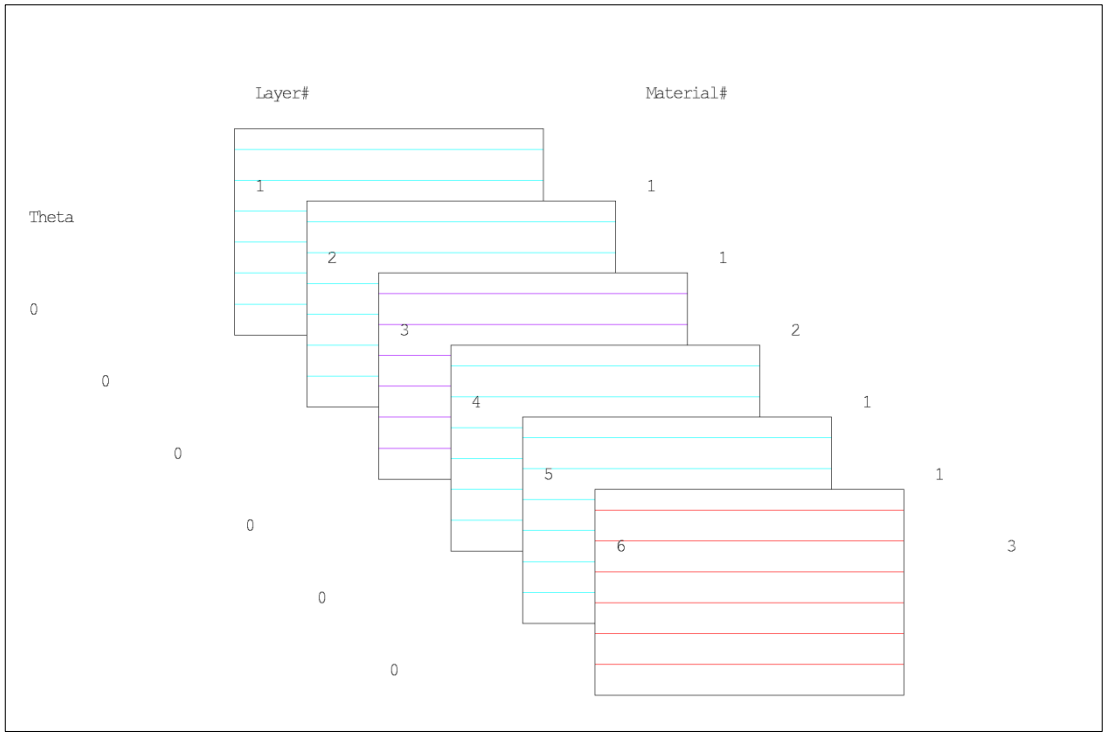

Figure 4. 17: The layers of the conical shell and text fixture.

4.5.4 Mesh lines

The cone is modeled by using 17280 eight nodded layered shell elements (Shell 281) and the text fixture is modeled by using 128 eight nodded layered shell elements. The root is fixed and the displacement is given to the tip of the cone. The finite element model is shown in Figure 4.18.

Before meshing, it is necessary:

- To select geometry to mesh
- To give a material type
- To give an element type
- To select to the mesh type (free or mapped meshing)
- To define the mesh refinement

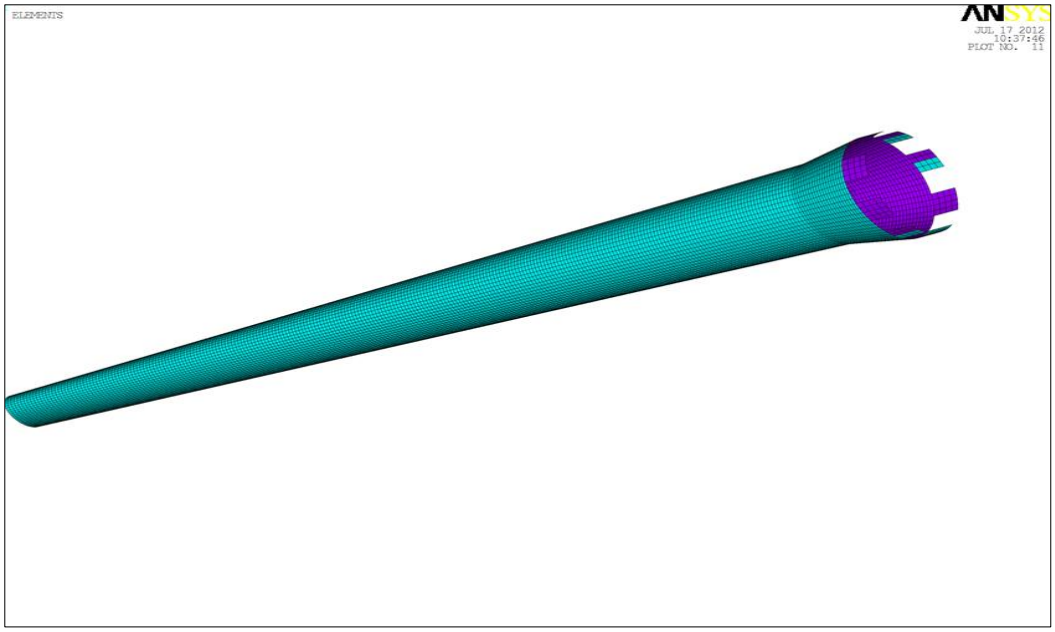

Figure 4. 18: The finite element model of the tail cone and test fixture.

4.5.5 Apply boundary conditions and load

The root is fixed and the displacement is given to the tip of the cone. The degrees of freedom of the root is set to 0. Figure 4.19 shows boundary conditions.

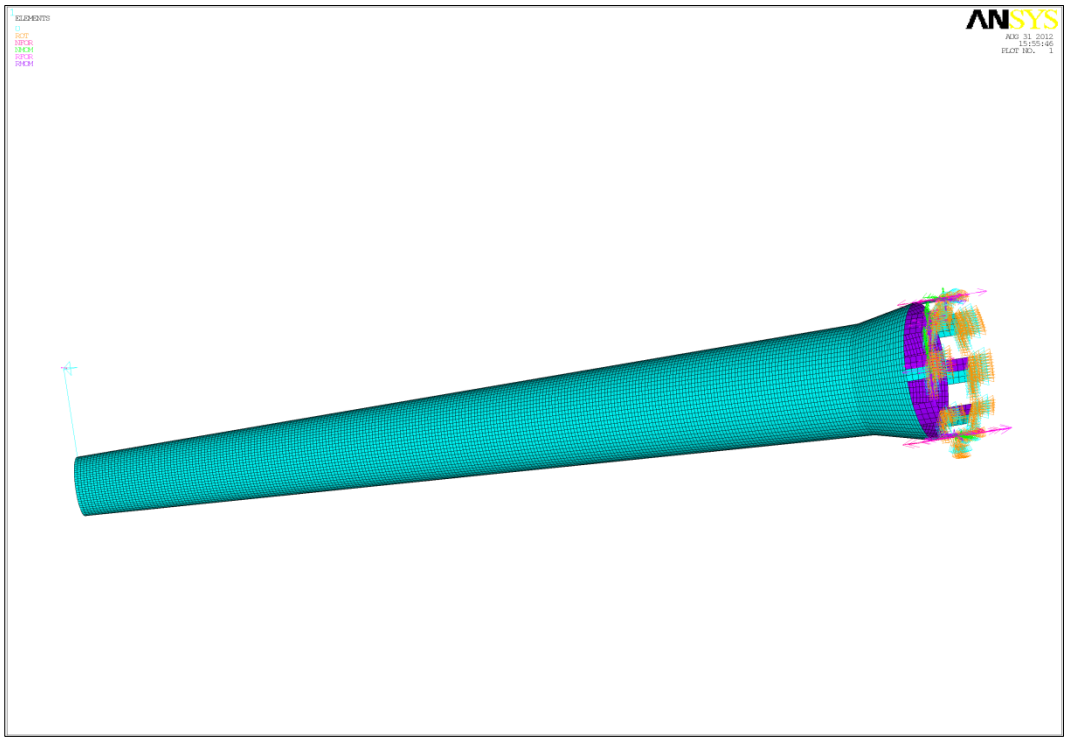

Figure 4. 19: Boundary conditions.

5. RESULTS AND DISCUSSIONS

5.1 Experimental Studies

In this thesis, mechanical and chemical tests were conducted by carbon fiber composite helicopter tail cone. Bidirectional carbon fiber is used for manufacturing an unmanned aerial vehicle.

The tail booms are the structure connecting the tail rotor to the fuselage. It is mainly subjected to the moment and torsion. Therefore, bending and torsional bending features were studied in this study. Built-in test mechanism has shown with Figure 5.1.

Figure 5.1: Built-in test mechanism.

According to the displacement of bending and torsional bending were performed on the MTS machine. Figure 5.2 and Figure 5.3 show bending and torsional bending test mechanism.

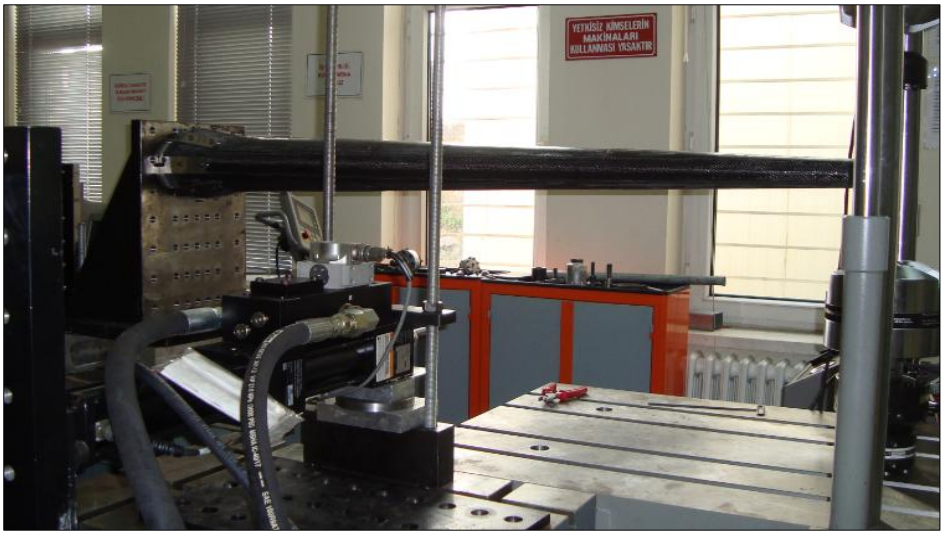

Figure 5. 2: Bending test mechanism.

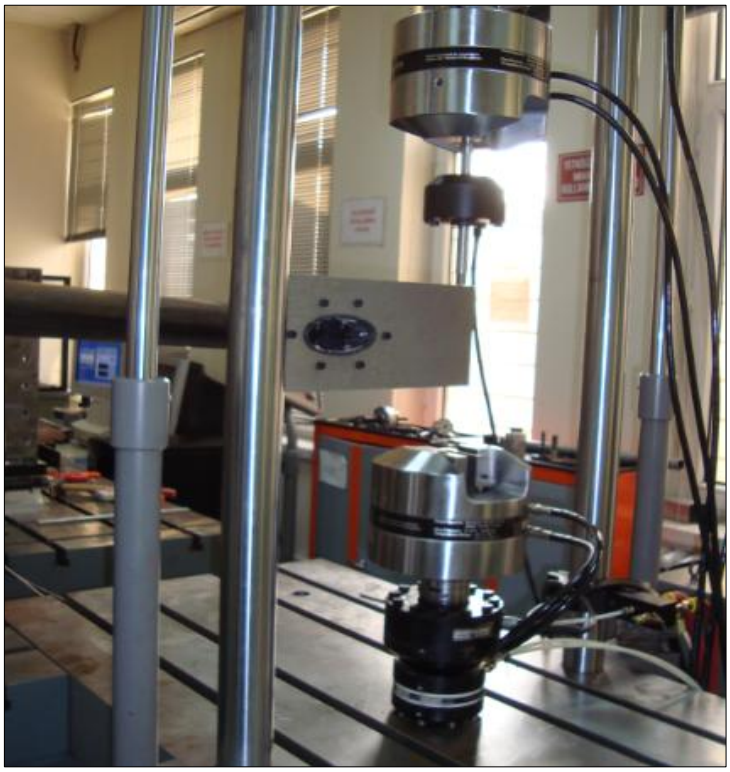

Figure 5.3: Torsional-bending test mechanism.

Each experiment was repeated three times. Experimental and numerical analysis results were compared with each other. The static analyses were achieved and the displacement field and stress distribution were obtained.

5.1.1 Bending test results

5 mm

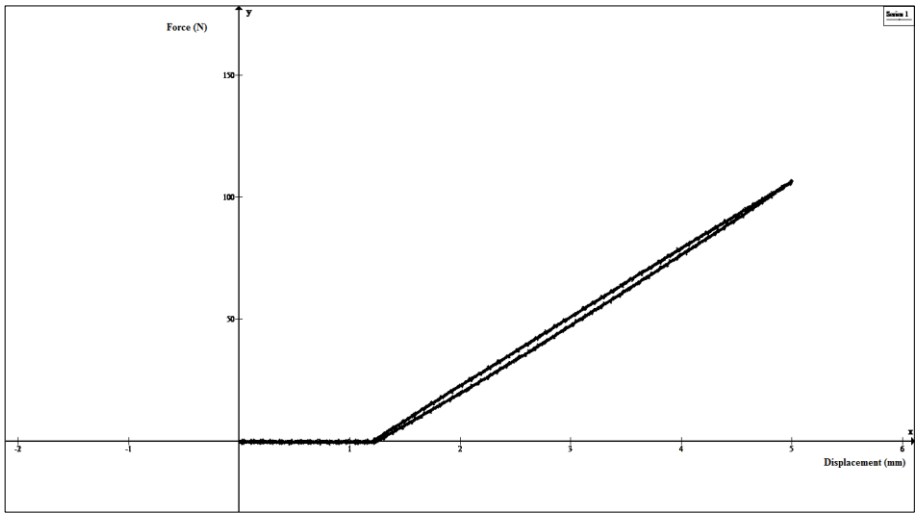

Figure 5.4: Bending test results for 5mm.

Figure 5.4 shows bending test results for 5 mm. Reaction force experimentally is 105 N.

10 mm

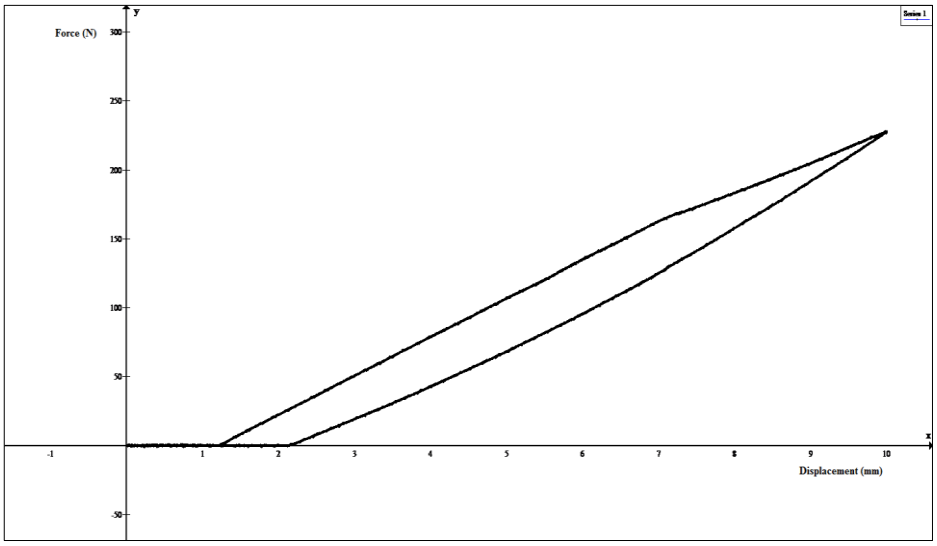

Figure 5.5: Bending test results for 10 mm.

Figure 5.5 shows bending test analysis for 10 mm. Reaction force experimentally is 228 N.

20 mm

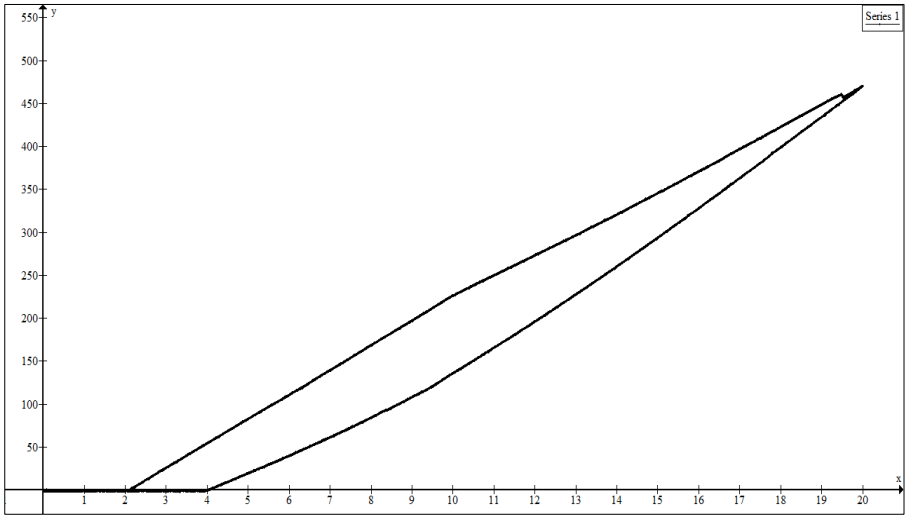

Figure 5.6: Bending test results for 20mm.

Figure 5.6 shows bending test results for 20 mm. Reaction force experimentally is 467 N.

5.1.2 Torsional-bending test results

20 mm

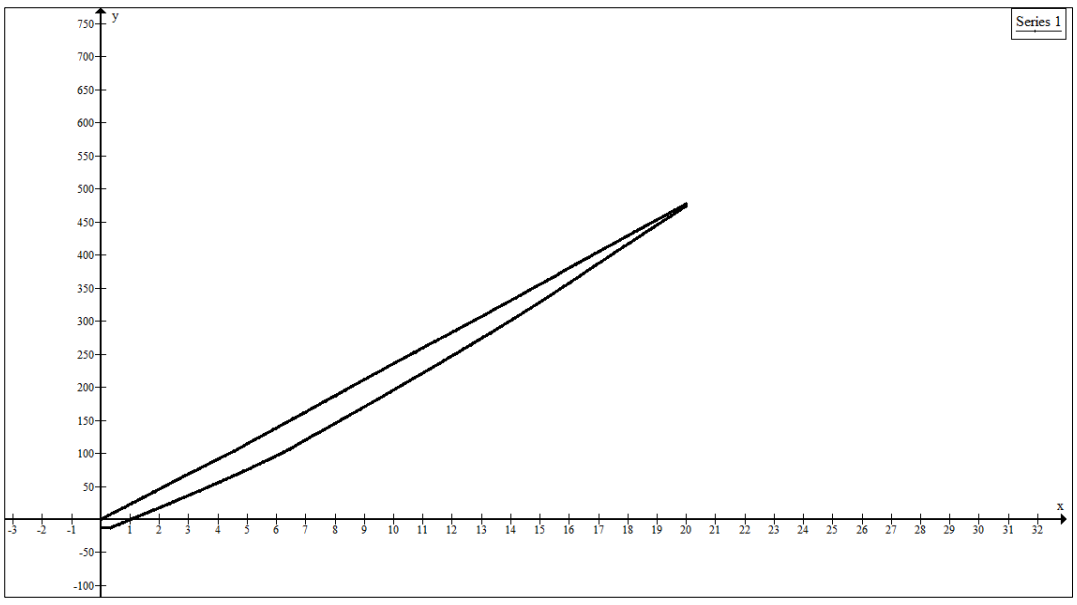

Figure 5.7: Torsional- bending test results for 20mm.

Figure 5.7 shows torsional-bending test results for 20mm. Reaction force experimentally is 474 N.

5.2 Finite Element Analysis of Helicopter Composite Tail Cone

5.2.1 Bending analysis of helicopter composite tail cone

Bending analysis for 5 mm

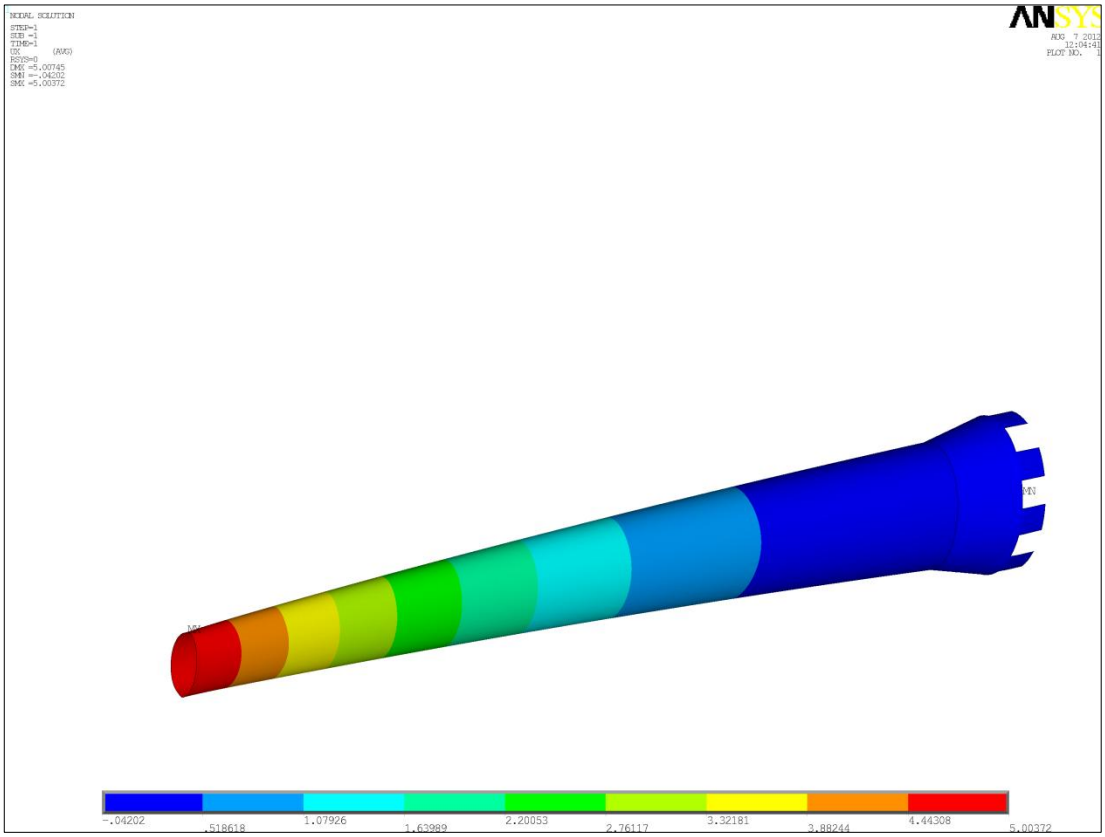

Figure 5.8: Displacement field of the bending analysis with 5 mm displacement applied at the tip of the tail cone.

A force in the negative direction of x axis is applied on the tail cone. Reaction force numerically is 103N. Figure 5.8 shows displacement field for 5 mm bending analysis.

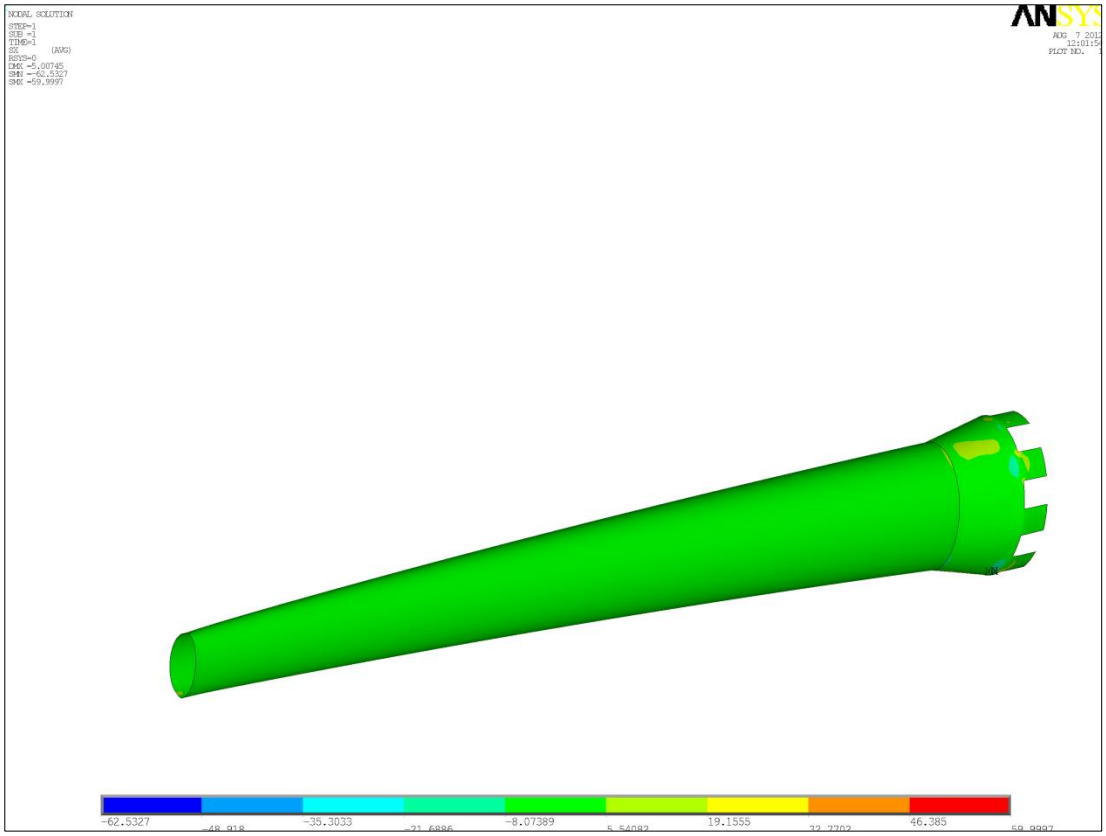

Figure 5. 9: Nodal stress field of the bending analysis with 5 mm displacement applied at the tip of the tail cone.

A force in the negative direction of x axis is applied on the tail cone. Nodal stress numerically is 59 MPa. Figure 5.9 shows nodal stress field for 5 mm bending analysis.

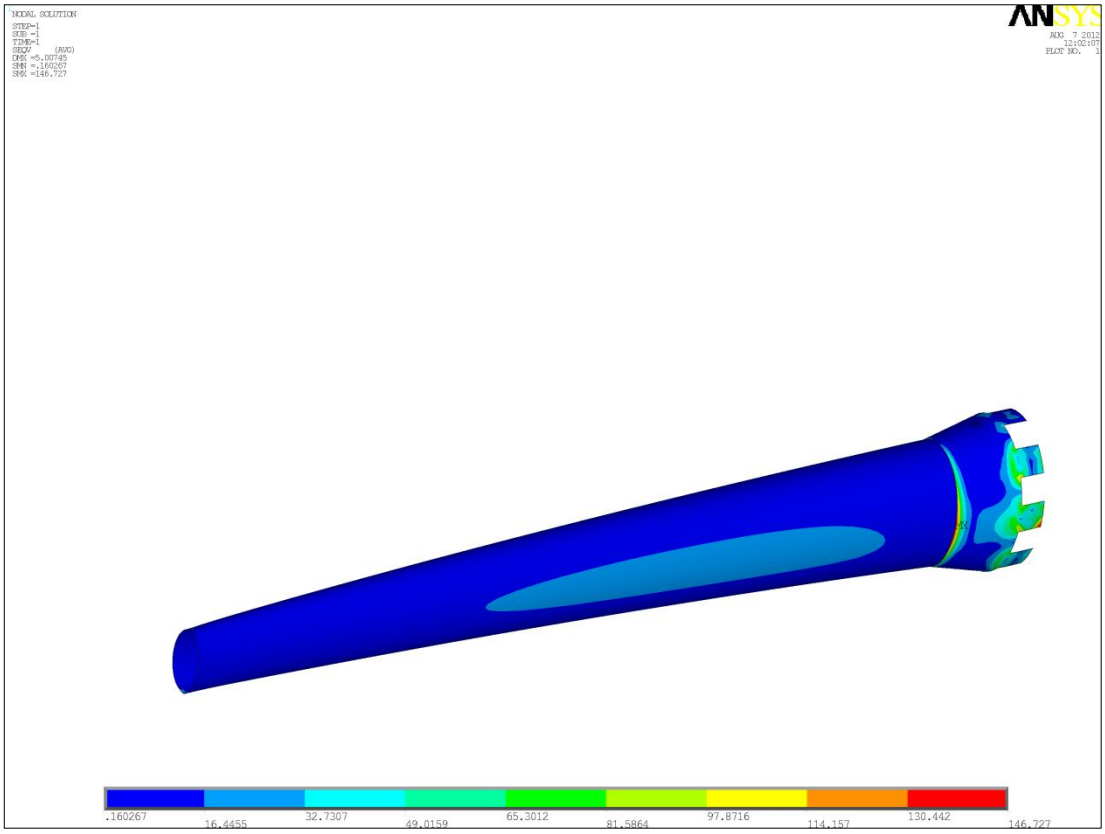

Figure 5. 10: Nodal Von-mises stress field of the bending analysis with 5 mm displacement applied at the tip of the tail cone

Nodal Von-mises stress numerically is 146MPa. Figure 5.10 shows nodal Von-mises stress for 5 mm bending analysis.

Bending analysis for 10 mm

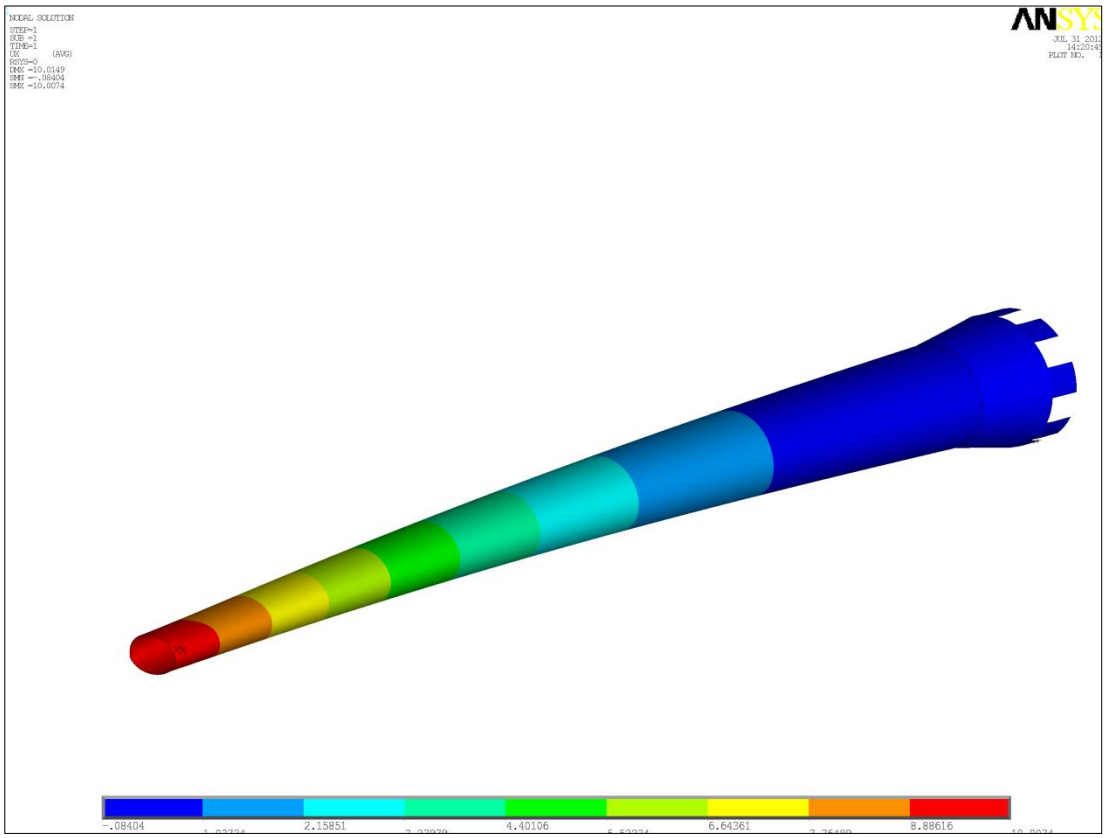

Figure 5.11: Displacement field of the bending analysis with 10 mm displacement applied at the tip of the tail cone.

Reaction force numerically is 207 N. Figure 5.11 shows displacement field for 10 mm bending analysis.

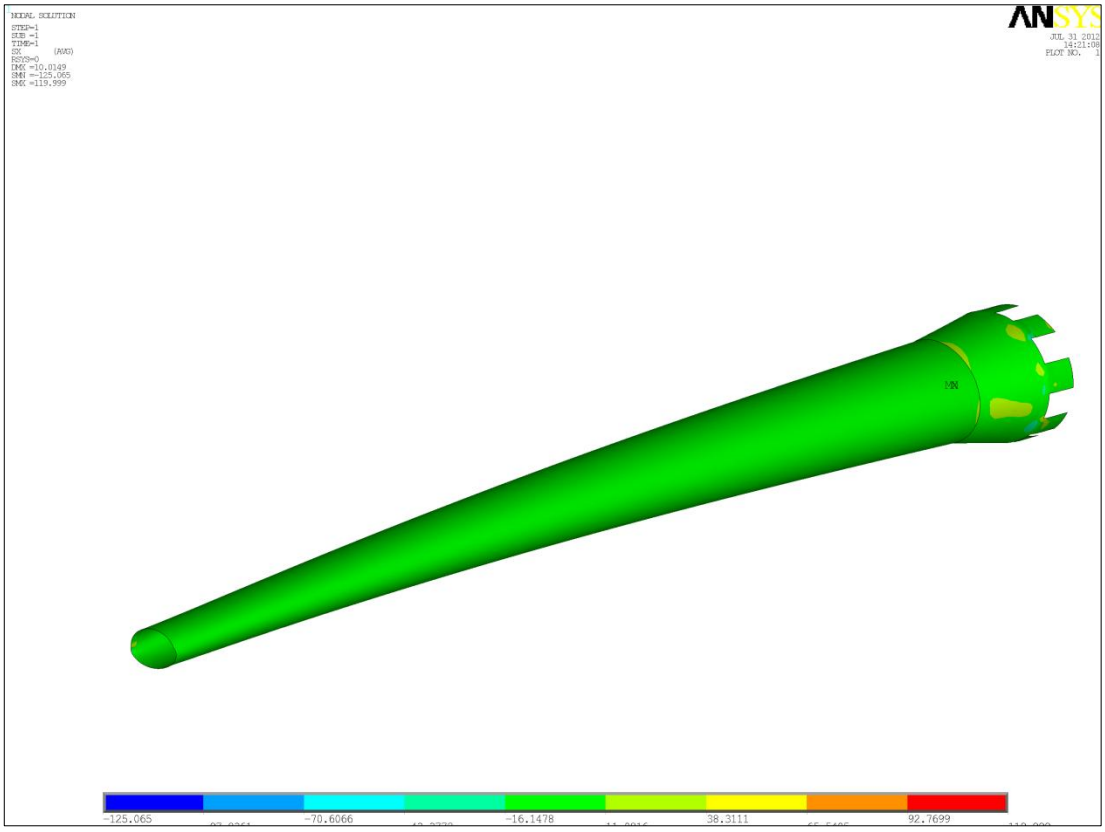

Figure 5. 12: Nodal stress field of the bending analysis with 10 mm displacement applied at the tip of the tail cone.

Nodal stress numerically is 119 MPa. Figure 5.12 shows nodal stress field for 10mm bending analysis.

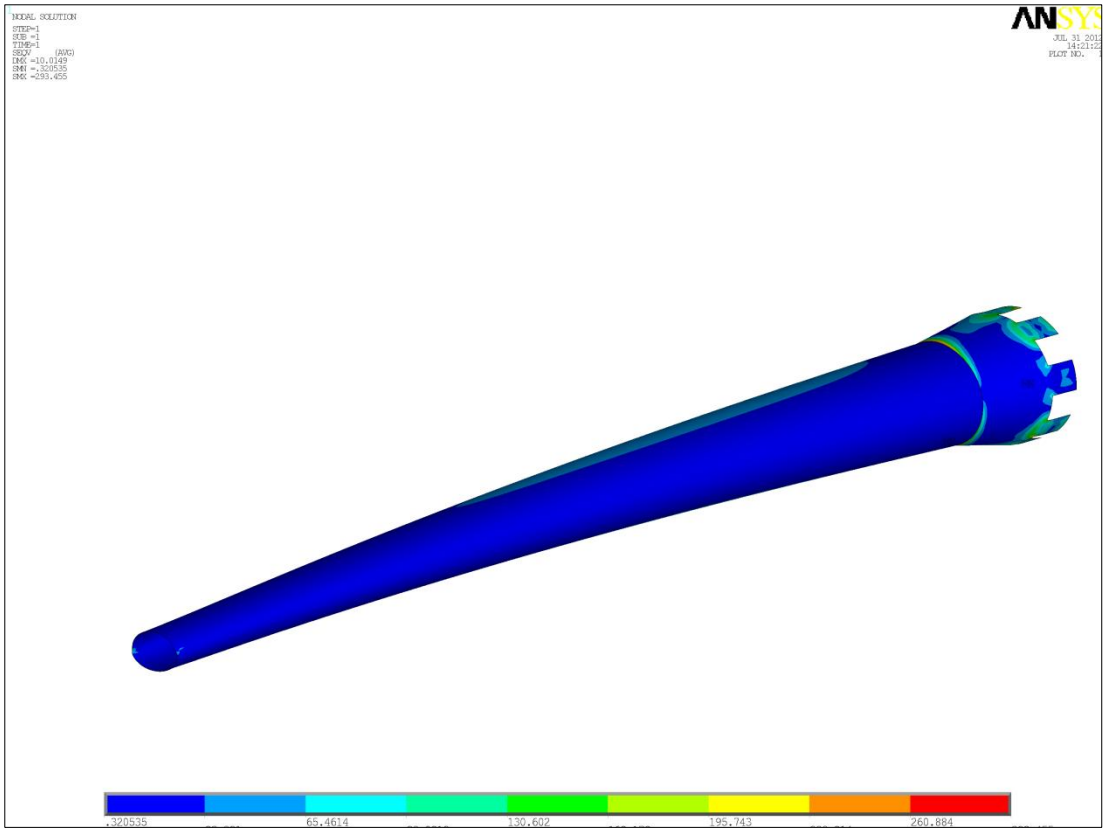

Figure 5.13: Nodal Von-mises stress field of the bending analysis with 10 mm displacement applied at the tip of the tail cone.

Nodal Von-mises numerically is 293 MPa. Figure 5.13 shows nodal Von-mises stress field for 10 mm bending analysis.

Bending analysis for 15 mm

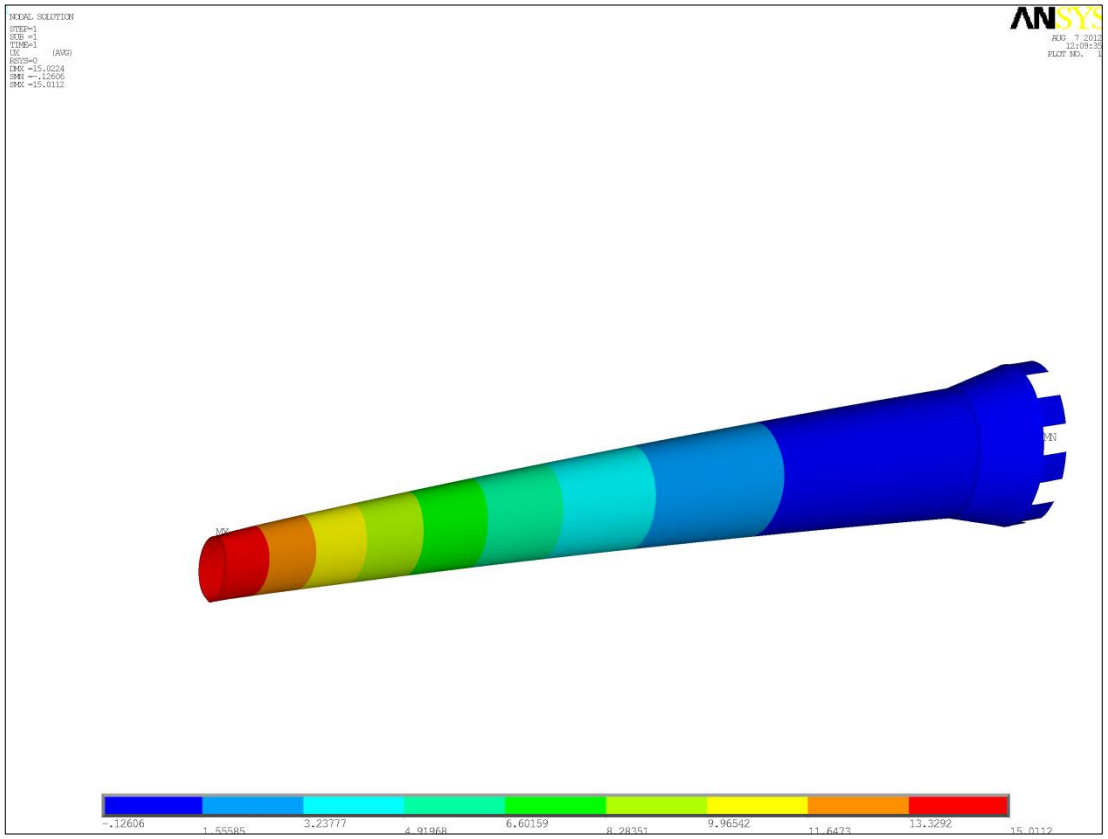

Figure 5. 14: Displacement field of the bending analysis with 15 mm displacement applied at the tip of the tail cone.

Reaction force numerically is 310 N. figure 5.14 shows displacement field for 15 mm bending analysis.

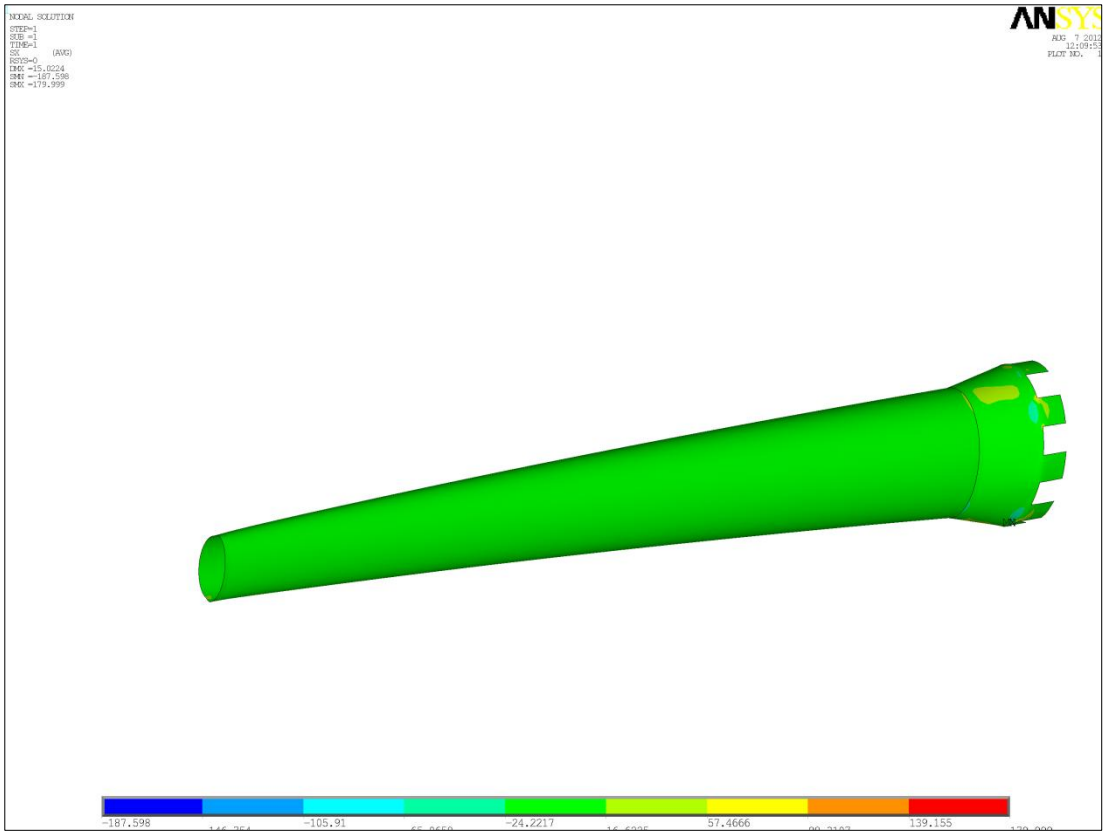

Figure 5. 15: Nodal stress field of the bending analysis with 15 mm displacement applied at the tip of the tail cone.

Nodal stress numerically is 179 MPa. Figure 5.15 shows nodal stress field for 15 mm bending analysis.

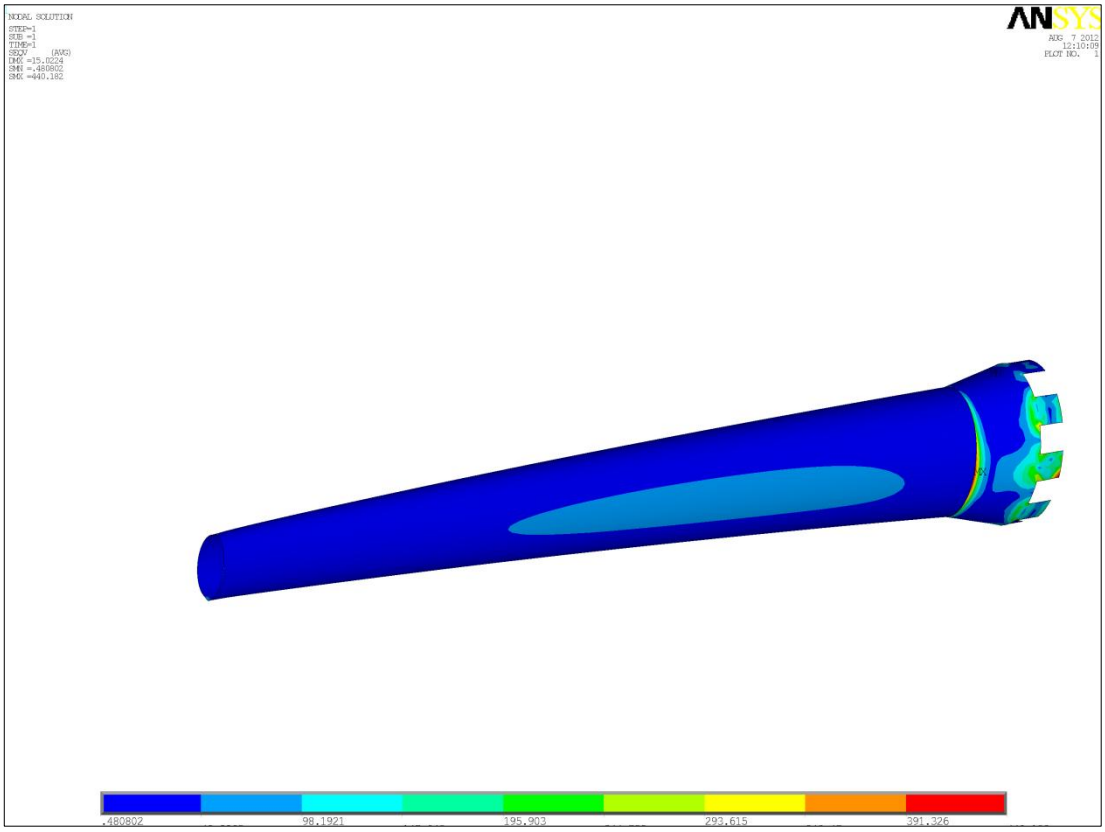

Figure 5. 16: Nodal Von-mises stress field of the bending analysis with 15 mm displacement applied at the tip of the tail cone.

Nodal Von-mises numerically is 440 MPa. Figure 5.16 shows nodal Von-mises stress field for 15 mm bending analysis.

Bending analysis for 20 mm

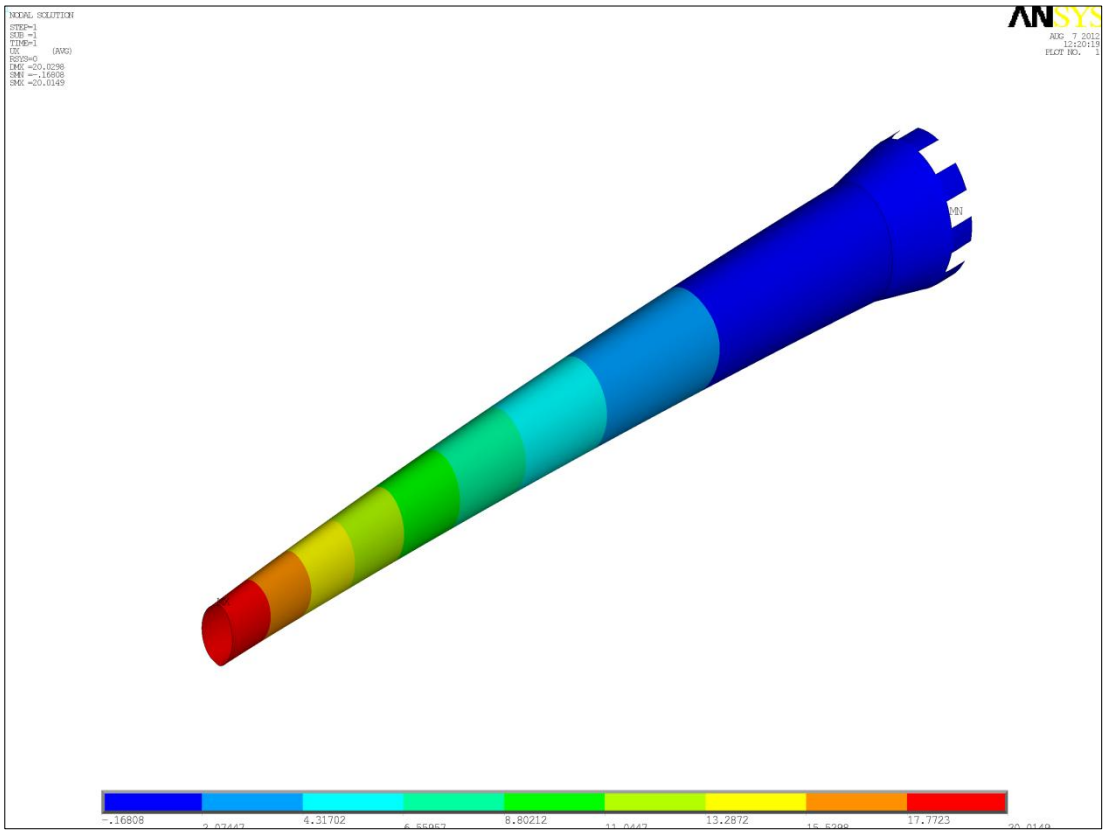

Figure 5.17: Displacement field of the bending analysis with 20 mm displacement applied at the tip of the tail cone.

Reaction force numerically is 414 N. Figure 5.17 shows displacement field for 20mm bending analysis.

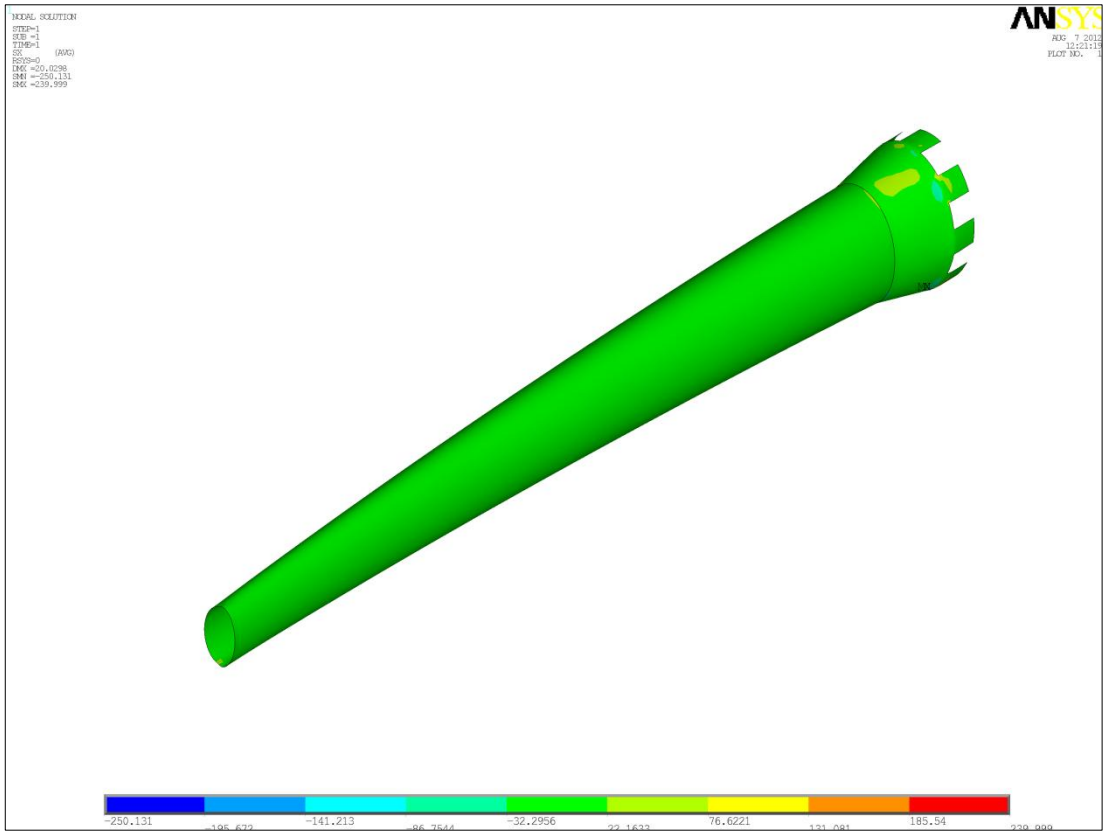

Figure 5. 18: Nodal stress field of the bending analysis with 20 mm displacement applied at the tip of the tail cone.

Nodal stress numerically is 239 MPa. Figure 5.18 shows nodal stress field for 20 mm bending analysis.

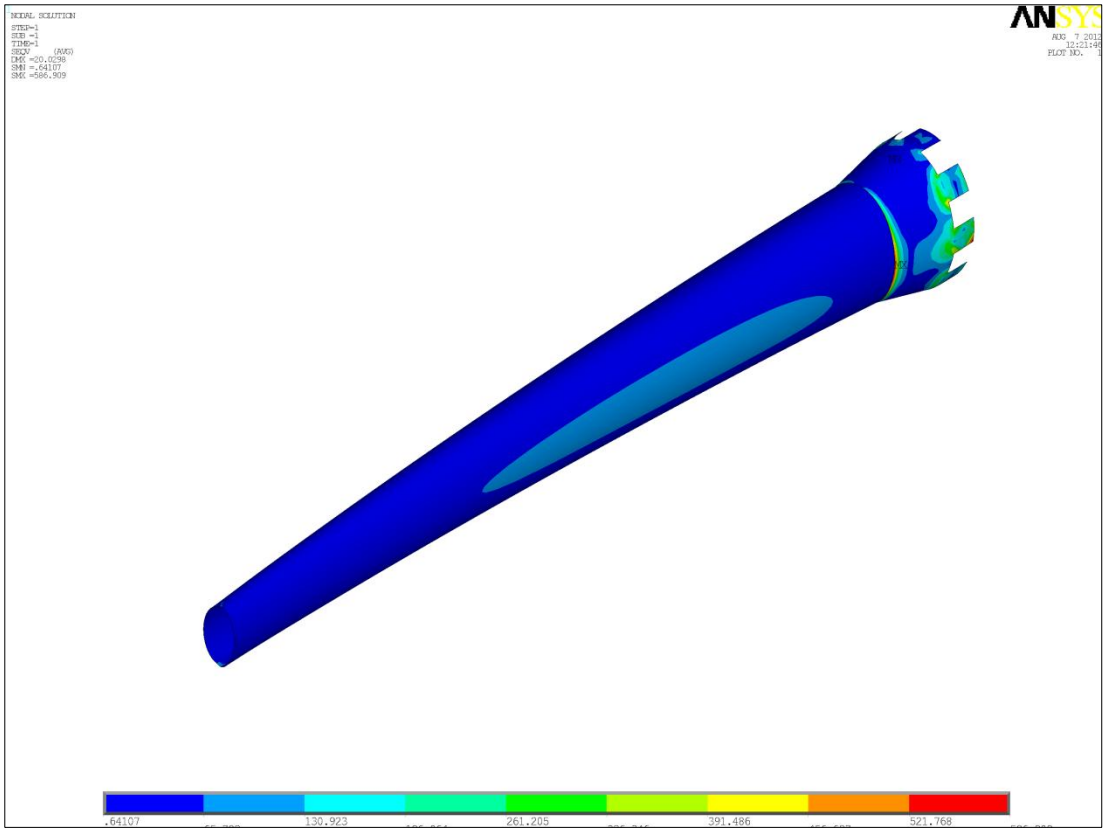

Figure 5. 19: Nodal Von-mises stress field of the bending analysis with 20 mm displacement applied at the tip of the tail cone.

Nodal Von-mises stress numerically is 586 MPa. Figure 5.19 shows nodal Von-mises stress field for 20mm bending analysis.

5.2.2 Torsional bending analysis of helicopter composite tail cone

Torsional-bending analysis for 5 mm

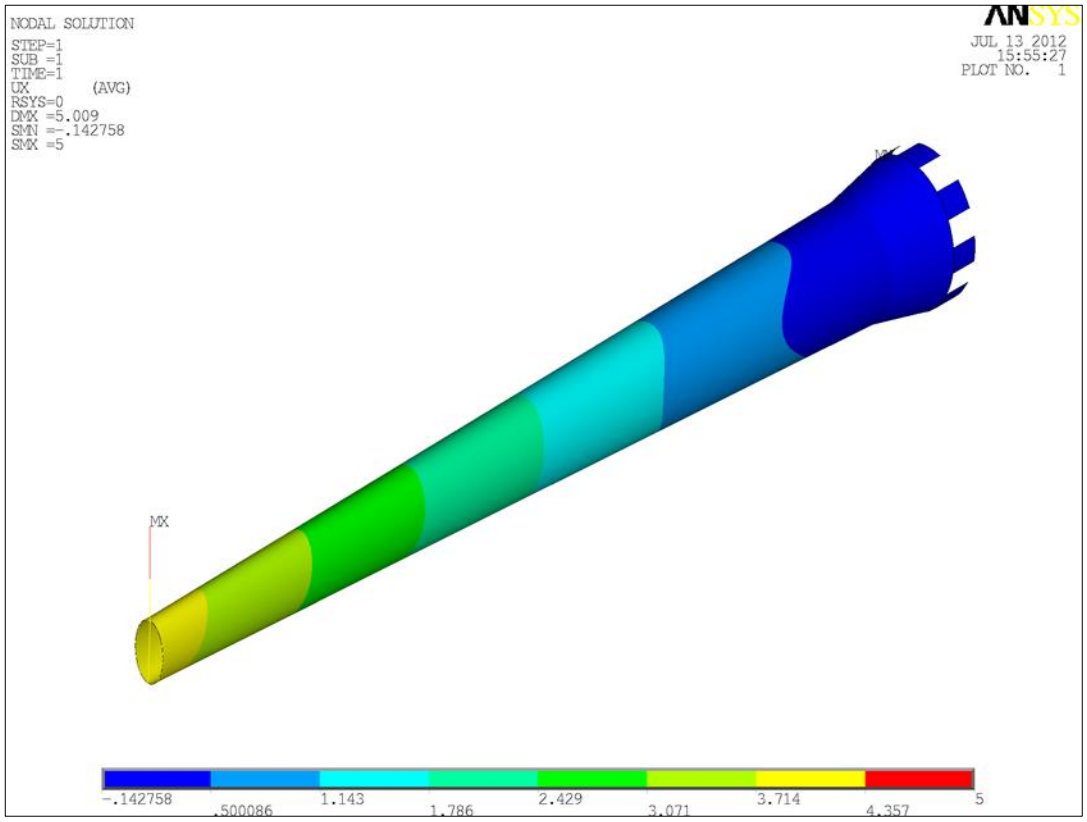

Figure 5.20: Displacement field of the torsional bending analysis with 5 mm displacement applied at the tip of the tail cone.

Reaction force numerically is 81 N. Figure 5.20 shows displacement field for 5 mm torsional bending analysis.

.

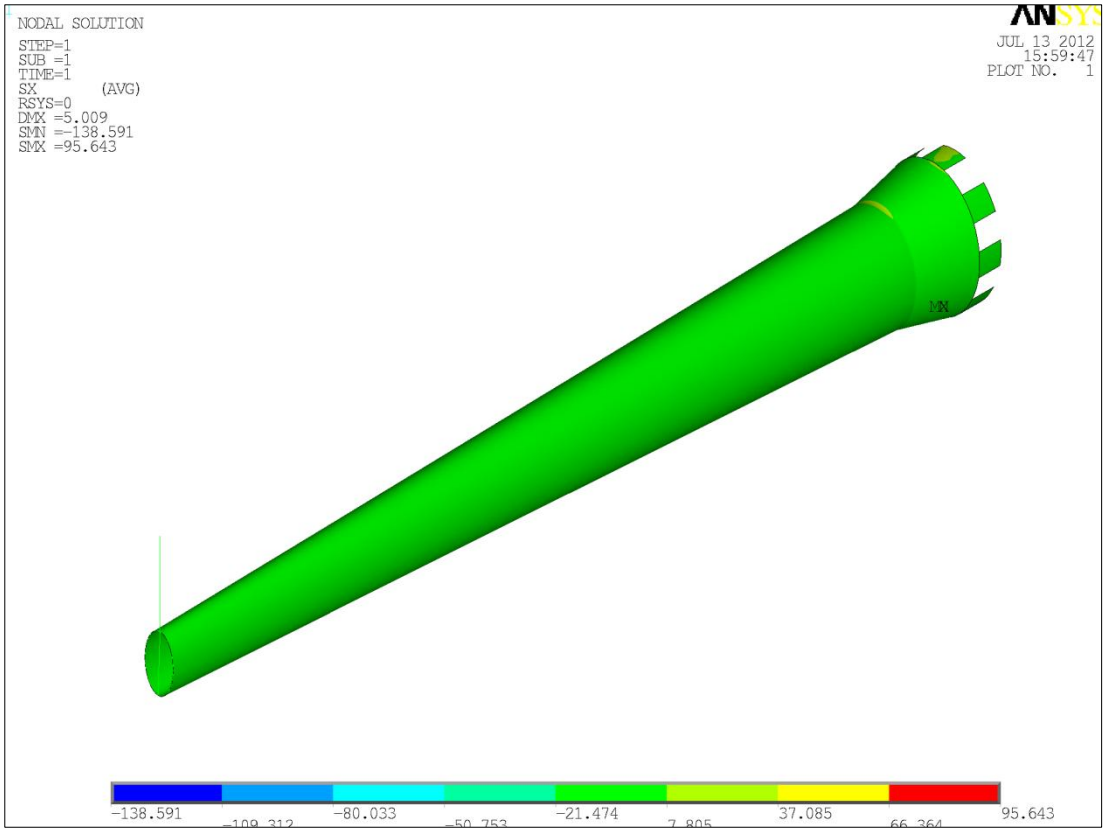

Figure 5.21: Nodal stress field of the torsional bending analysis with 5 mm displacement applied at the tip of the tail cone.

Nodal stress numerically is 95 MPa. Figure 5.21 shows nodal stress field for 5 mm torsional bending analysis.

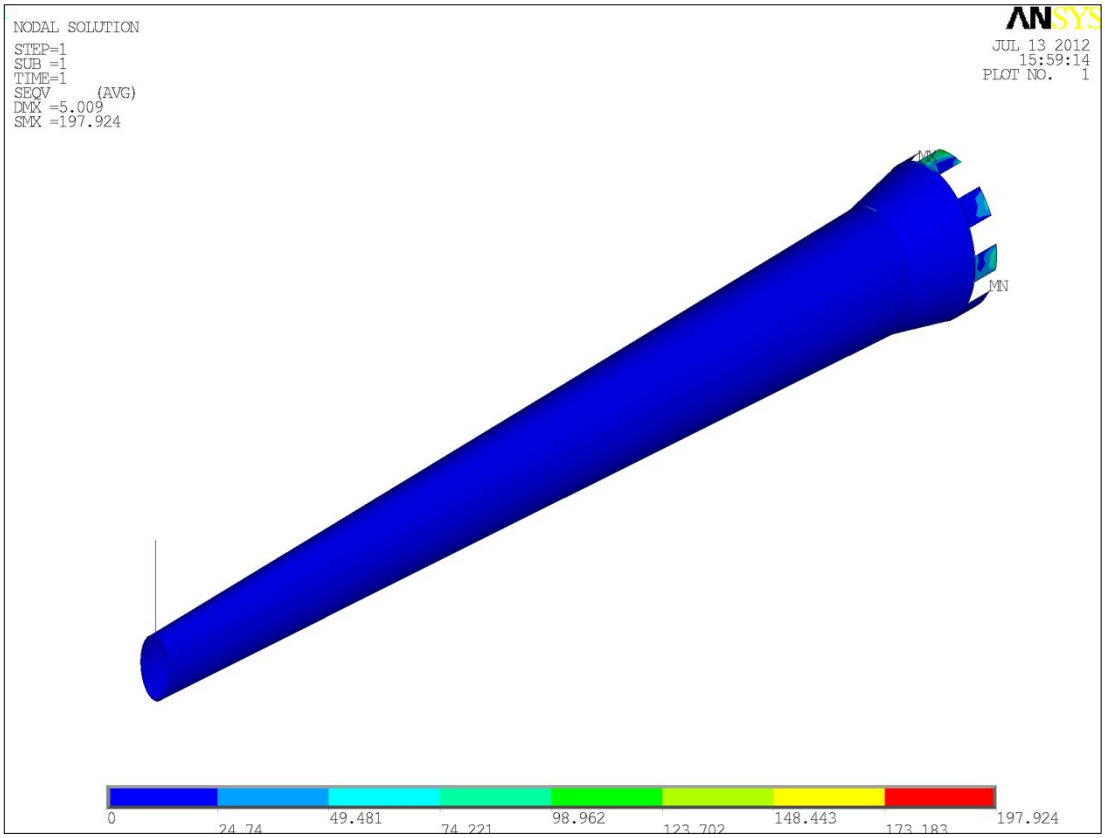

Figure 5.22: Nodal Von-mises stress field of the torsional bending analysis with 5 mm displacement applied at the tip of the tail cone.

Nodal Von-mises stress numerically is 197 MPa. Figure 5.22 shows nodal Von-mises stress for 5 mm torsional bending analysis.

Torsional-bending analysis for 10 mm

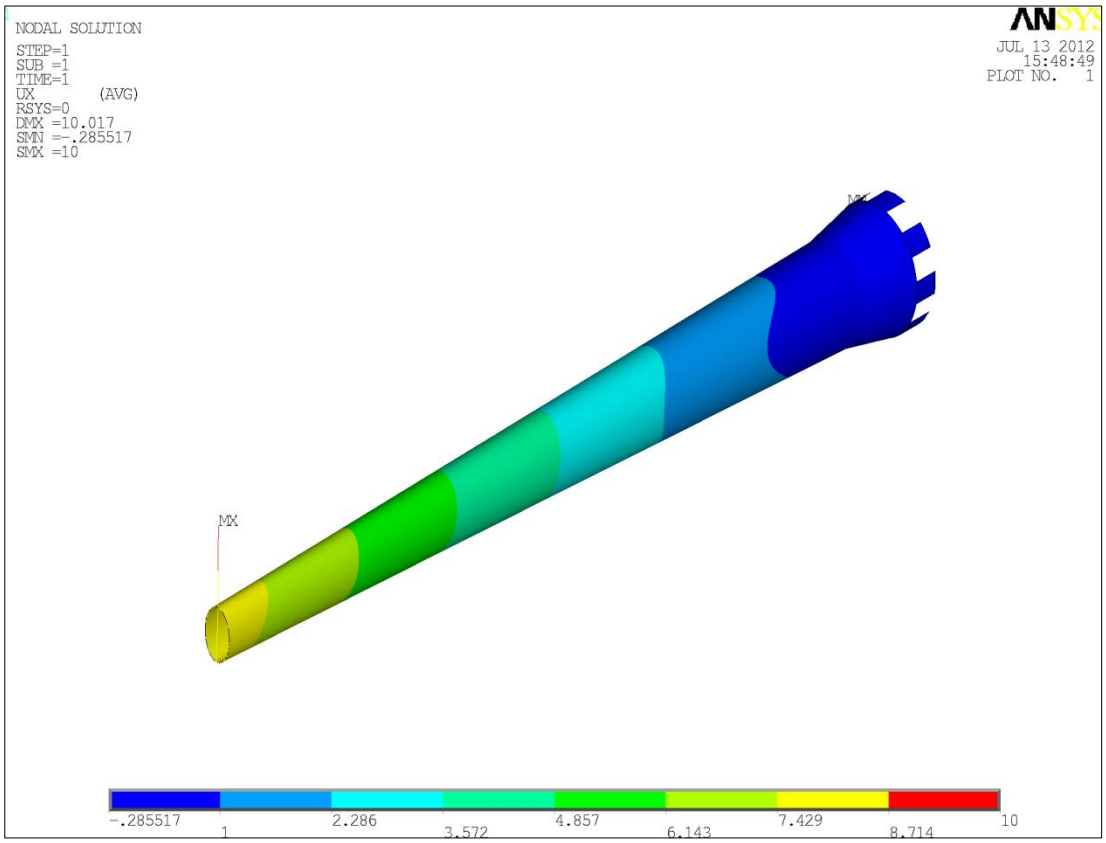

Figure 5.23: Displacement field of the torsional bending analysis with 10 mm displacement applied at the tip of the tail cone.

Reaction force numerically is 162 N. Figure 5.23 shows displacement field for 10 mm torsional bending analysis.

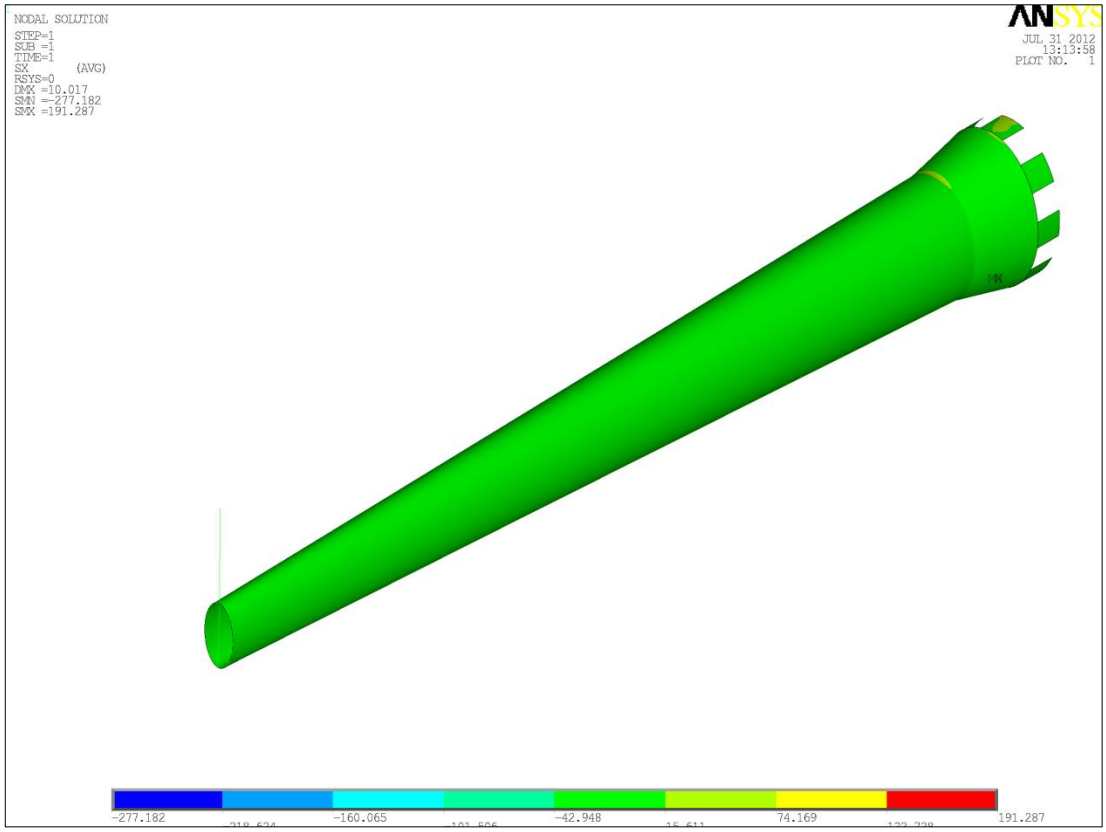

Figure 5.24: Nodal stress field of the torsional bending analysis with 10 mm displacement applied at the tip of the tail cone.

Nodal stress numerically is 191MPa. Figure 5.24 shows nodal stress field for 10 mm torsional bending analysis.

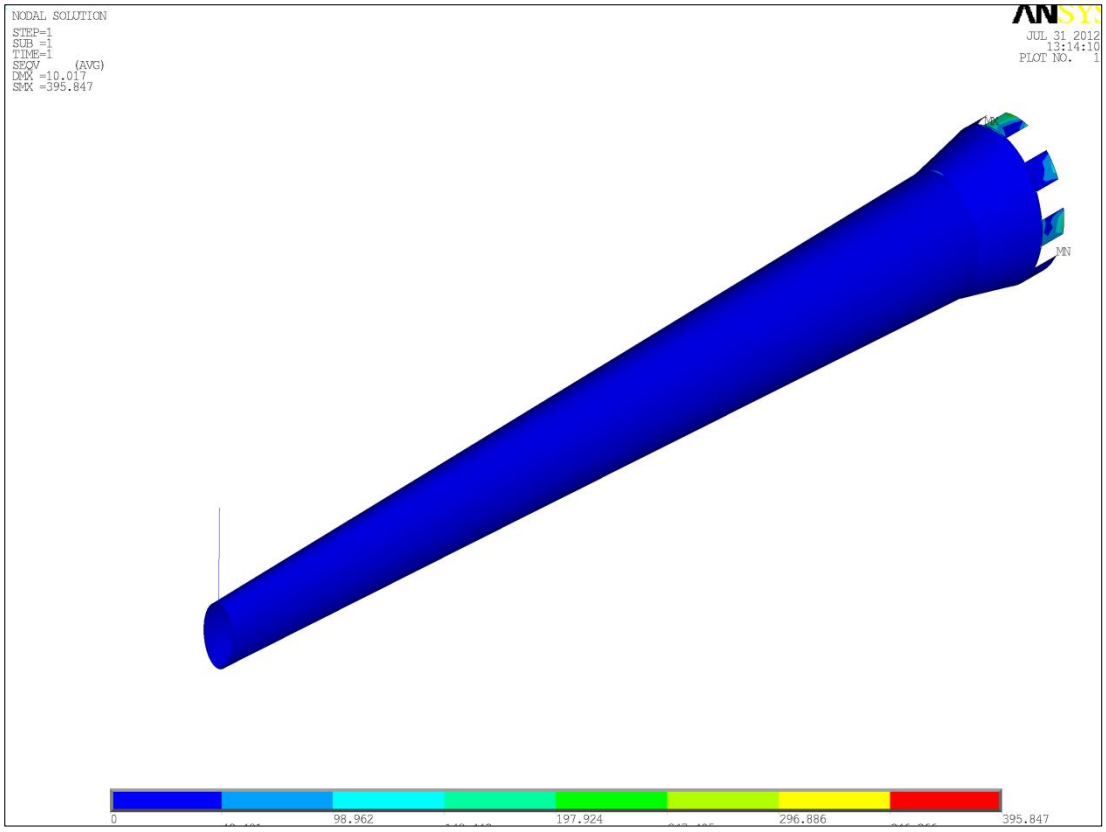

Figure 5.25: Nodal Von-mises stress field of the torsional bending analysis with 10 mm displacement applied at the tip of the tail cone.

Nodal Von-mises stress numerically is 395MPa. Figure 5.25 shows nodal Von-mises stress field for 10 mm torsional bending analysis.

Torsional-bending analysis for 15 mm

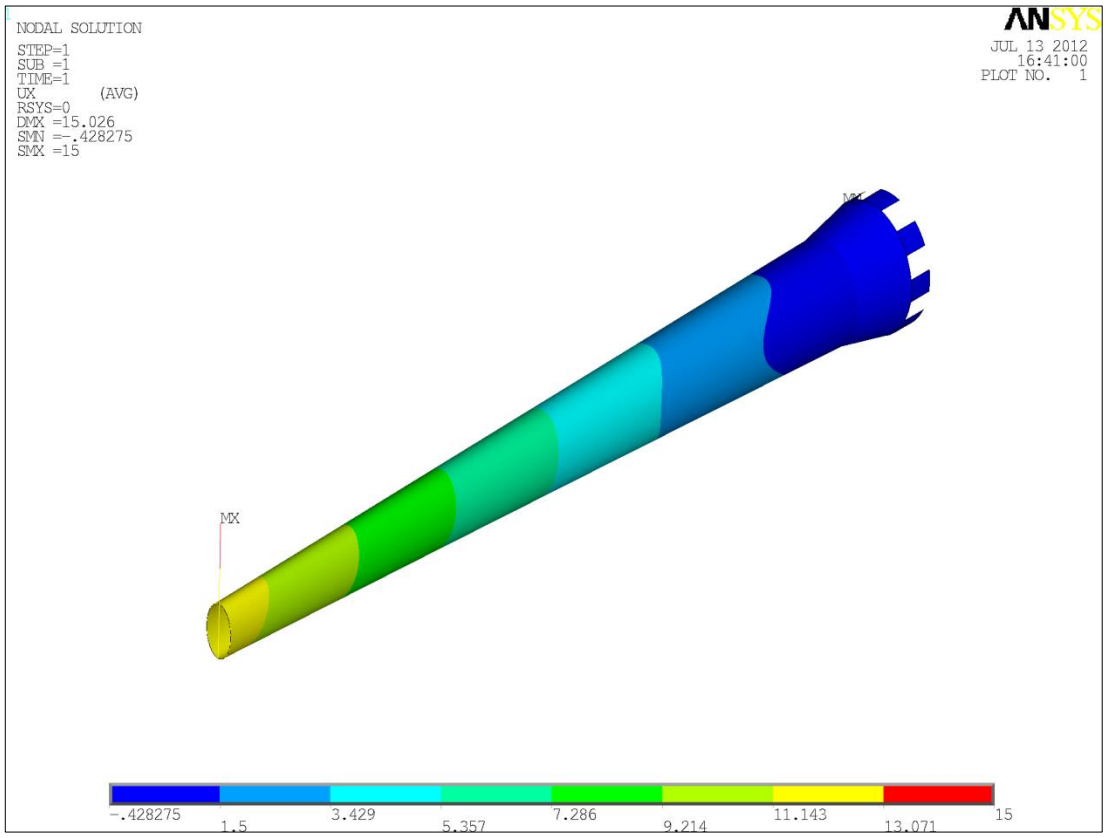

Figure 5.26: Displacement field of the torsional bending analysis with 15 mm displacement applied at the tip of the tail cone.

Reaction force numerically is 243 N. Figure 5.26 shows displacement field for 15 mm torsional bending analysis.

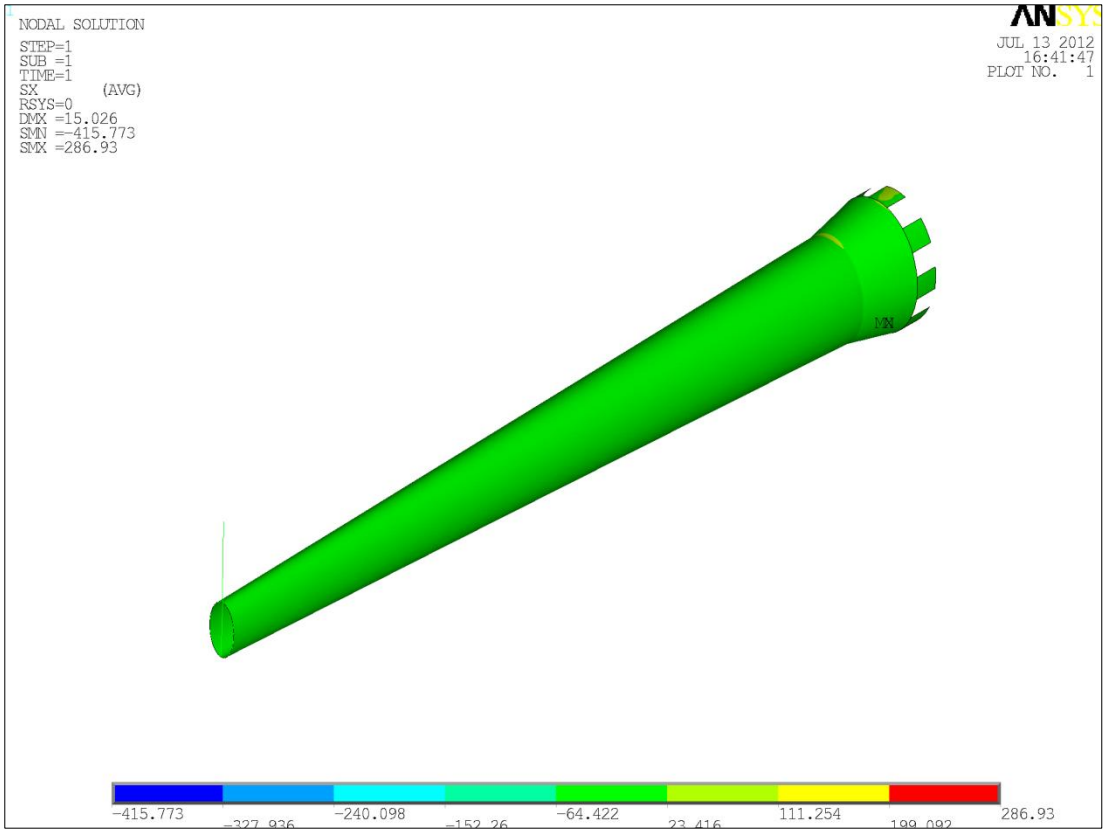

Figure 5.27: Nodal stress field of the torsional bending analysis with 15 mm displacement applied at the tip of the tail cone.

Nodal stress numerically is 286 MPa. Figure 5.27 shows nodal stress field for 15 mm torsional bending analysis.

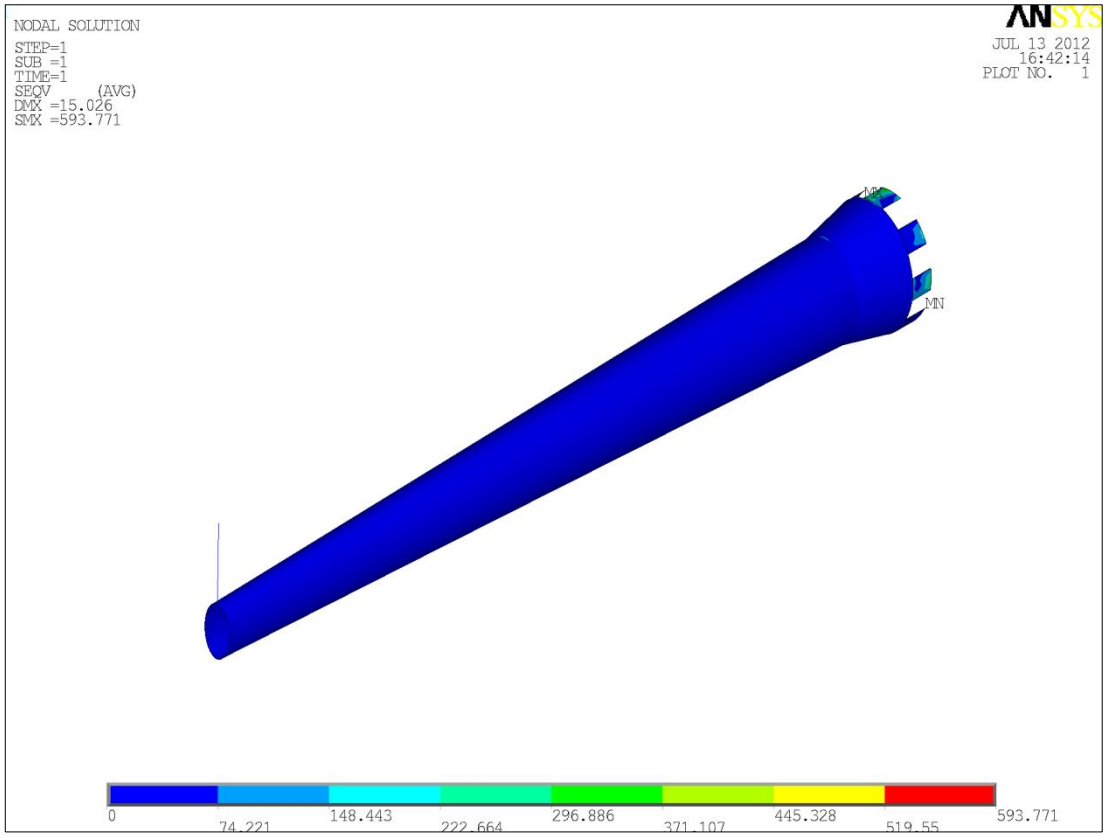

Figure 5.28: Nodal Von-mises stress field of the torsional bending analysis with 15 mm displacement applied at the tip of the tail cone.

Nodal Von-mises numerically is 593 MPa. Figure 5.28 shows nodal Von-mises stress field for 15 mm torsional bending analysis.

Torsional-bending analysis for 20 mm

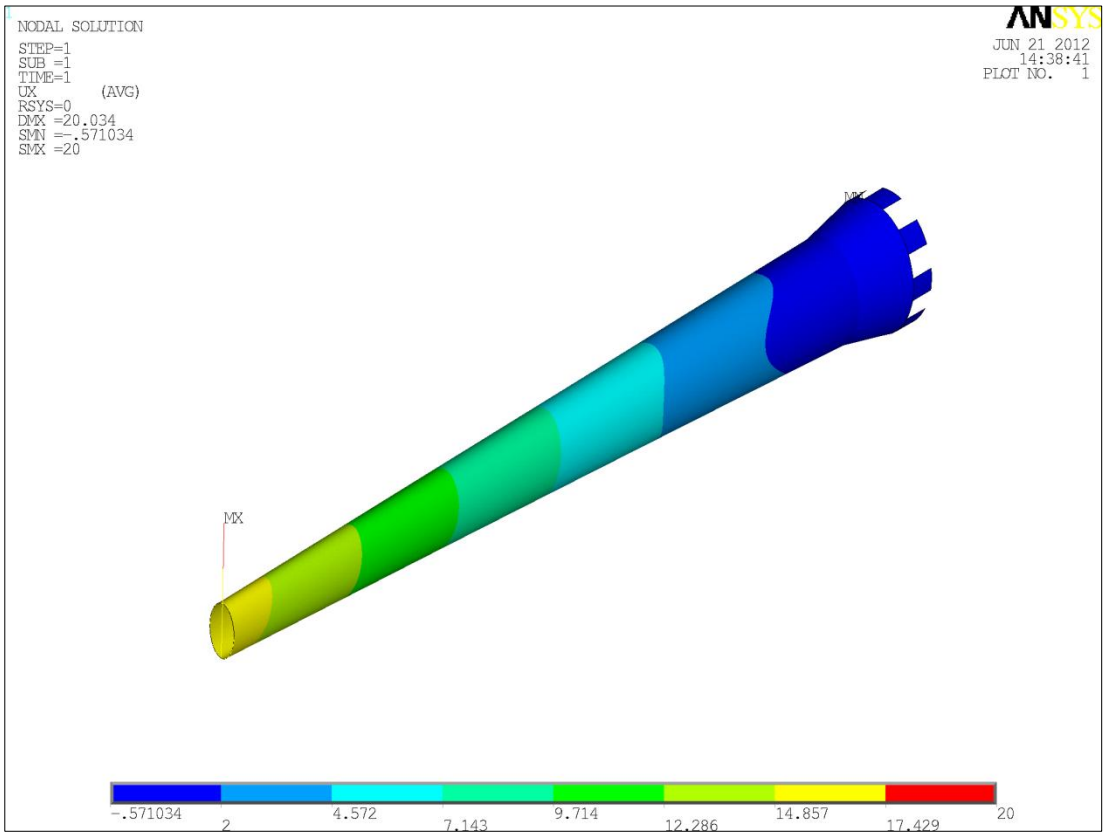

Figure 5.29: Displacement field of the torsional bending analysis with 20 mm displacement applied at the tip of the tail cone.

Reaction force numerically is 324 N. Figure 5.29 shows displacement field for 20 mm torsional bending analysis.

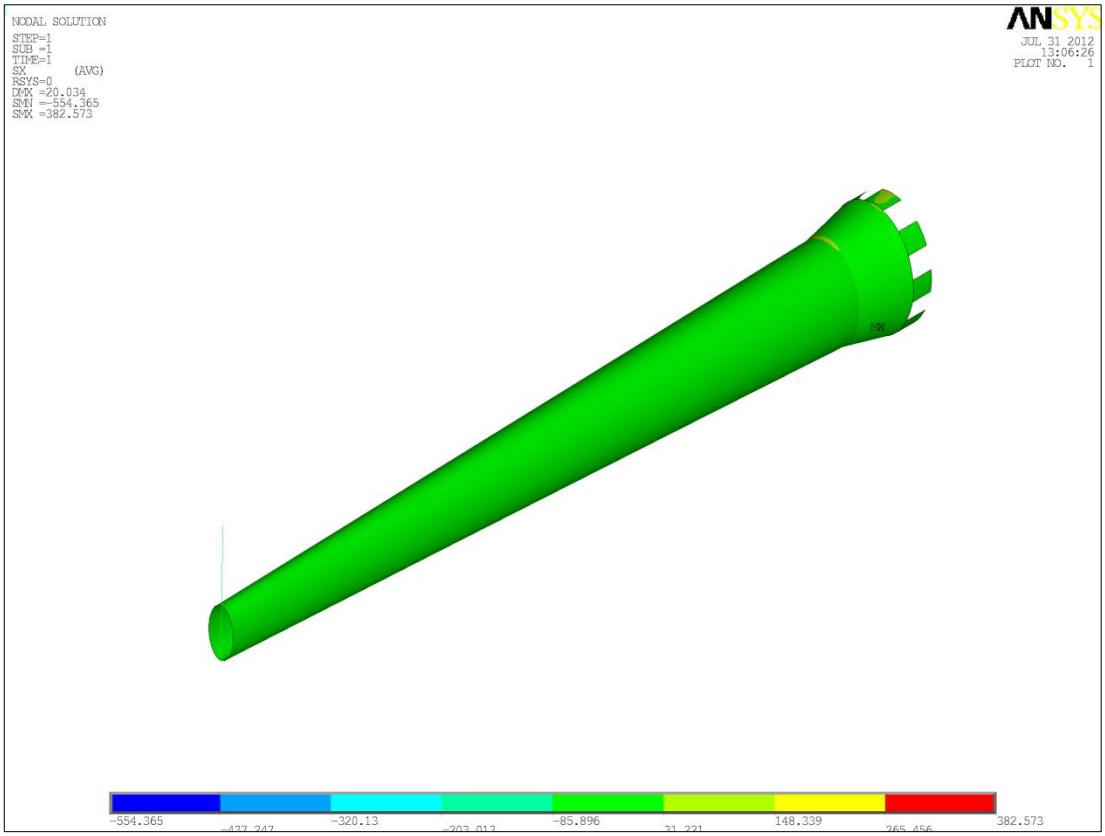

Figure 5.30: Nodal stress field of the torsional bending analysis with 20 mm displacement applied at the tip of the tail cone.

Nodal stress numerically is 382 MPa. Figure 5.30 shows nodal stress field for 20 mm torsional bending analysis.

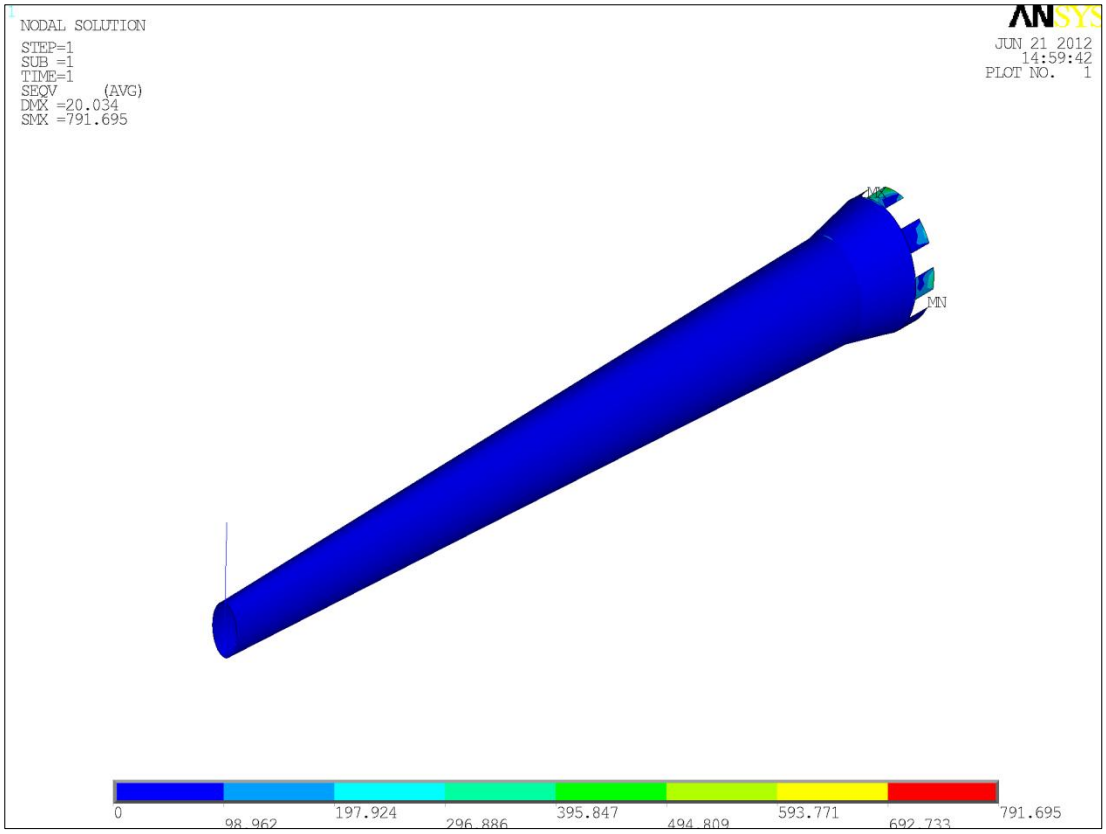

Figure 5.31: Nodal Von-mises stress field of the torsional bending analysis with 20 mm displacement applied at the tip of the tail cone.

Nodal Von-mises numerically is 791 MPa. Figure 5.31 shows nodal Von-mises field for 20 mm torsional bending analysis.

To sum up, all test results and static analysis results are given in Table 5.1.

Table 5. 1: Experimental and numerical reaction force.

Displacement (mm)	Reaction Force (N) Experimental	Reaction Force (N) Numerical
Bending		
5	143	103
10	292	207
15	438	310
20	575	414
Torsional-Bending		
5	115	81
10	236	162
15	356	243
20	474	324

Special note: All reaction forces experimentally were taken from 20 mm displacement experiment in Table 5.1.

The tail boom is modeled by using ANSYS finite element software and static analyses are achieved. Experimental and static analyses are consistent each other.

5.3 Discussion

In this thesis, firstly two kinds of helicopter composite model tail cone were produced with hand lay-up technique. Optimum weight and bending and torsional-bending properties were investigated for models of tail cone structure. Thus, optimization can be performed by maximization of the load for the specific weight, or by minimization of the weight of the structure the constraint of applied load. After that, optimum features were investigated and then original composite tail cone was produced in same conditions.

An unmanned helicopter tail boom was manufactured with honeycomb between 4-plies carbon fiber. Bending and torsional bending features were investigated both numerical and experimental. The measured and computed reaction forces were shown Table 5.1. It is shown that the reaction force is higher for the bending

compared to the torsional bending . This is because the torsional reaction moment is also contributing the load carrying in the case of torsional bending. The predicted reaction forces are found to be approximately 30% lower than the measured ones. The material properties used in the analysis could be a reason for this discrepancy. Also, the assumptions in modeling the boundary conditions could be a reason for the discrepancy.

The result of DSC analysis is compatible with technical information of Hexion L285 epoxy. According to DSC analysis in İTÜ Polymer Laboratory, the glass transition event, T_g, is observed at 0 °C as an exothermic stepwise increase. The endothermic peak temperature reflects the maximum rate of curing of the resin. The endothermic peak temperature is 58.45° C as shown in Figure 4.3. Therefore, composite semi-conical shells must be produced in 60ºC.

Furthermore, carbon fiber composite material was analyzed with Bruker D8 Advance X-ray diffractometer in İTÜ. According to İTÜ PML Laboratory, XRD diffraction study is similar to previous studies. Carbon fiber composite diffraction degree is approximately 26º.

REFERENCES

[1]**Ajit Shingh**.(2001).Radiation Processing of Carbon Fibre-Reinforced Advanced Composites:AHA Enterprises, 82 Gulfview Place, Victoria, BC, Canada V8Y 2R6.

[2]**M. Hasan, M. E. Hoque, and S. M. Sapuan. (2010).** Composite Material Technology- Neural Network Applications**.**

[3]**Brian Cantor, Hazel Assender, Patrick Grant.** (2001). Department of Materials, University of Oxford, UK; Aerospace Materials; 2001 IOP Publishing Ltd.

[4]http://www.helis.com/introduction/prin.php>03.04.2012

[5]http://www.marinecomposites.com/PDF_Files/f_aerospace_applications.pdf>12.04.2012

[6]P-023N Advanced Polymer Matrix Composites, Business Communication Company, Inc.

[7]**A Mouritz.** Introduction to aerospace materials, Royal Melbourne Institute of Technology, Australia.

[8]**Brian Cantor and Fionn Dunne and Ian Stone**. (2004) Metal and Ceramic Matrix Composites. The University of York and The University of Oxford, UK.

[9]**John Watkinson**.(2004) Art of Helicopter, Pages: 166-190.

[10]**L. Molent.** (1995) Structural and Flight Trial Analysis in Support of AS-350 Squirrel Helicopter Tail Cone Buckling. Aeronautical and Maritime Research Laboratory Airfraims and Engine Division.

[11]http://www.nindadesign.com/projects.html>21.01.2012

[12]**Marc E . Tuttle.** (2003). Structural Analysis of Polymeric Composite Materials, CRC Press.

[13]**Sanjay K.Mazlumdar,Ph.D.** (2002). Composite Manufacturing, Materials, Product and Process Engineering.

[14]**A.Brent Strong.** History of Composite Materials, Opportunities and Necessities. Brigham Young University.

[15]**Autar K.Kaw.** (2006). Mechanics of Composite Materials.

[16]**N.Chawla, K.K. Chawla.** (2009). Metal Matrix Composites.

[17]**Rajindal Pal.** New models for effective Young's modulus of particulate composites

[18]**Zafer Gürdal, Raphael T. Haftka, Praphat Hajela.** Design and Optimization of Laminated Composite Materials.

[19]http://www.ccm.udel.edu/Tech/Lam3D/Theory.htm>02.05.2012

[20]**Hota V. S. GangaRao, Narendra Taly, P. V. Vijay**. (2007) Reinforced Concrete Design with FRP Composites book.

[21 http://www.pultrusions.org/articles/pultrusion_works.html>15.03.2012

[22]**A. R. Bunsell J Renard.** (2005). Fundamentals of Fibre Reinforced Composite Materials.

[23]http://www.substech.com/dokuwiki/doku.php?id=compression_molding_of_polymers.>24.03.2012

[24]**SoonKook Hong**.(2010). Assessment of Durability of Carbon/Epoxy Composite Materials after Exposure to Elevated Temperatures and Immersion in Seawater for Navy Vessel Applications. A Dissertation submitted in partial satisfaction of the Requirements for the degree of Doctor of Philosophy In Materials Science and Engineering.

[25]**W.J. Sichina.(2000).** Characterization of Epoxy Resins Using DSC.

[26]**Barbara L Dutrow.** Louisiana State University , Christine M. Clark, Eastern Michigan University.

[27]**T. Nishino, H. Naito, K. Nakamura, K. Nakamae**.(2000).X-ray diffraction studies on the stress transfer of transversely loaded carbon fibre reinforced composite.

[28]ANSYS 13 User Manual, ANOVA.

CURRICULUM VITAE

Name Surname: Deniz KAVRAR

Place and Date of Birth: İstanbul/ 09 May 1987

E-Mail: dkavrar@itu.edu.tr

B.Sc.: İstanbul University / Deparment of Metallurgy and Materials Engineering 2009.

PUBLICATIONS/PRESENTATIONS ON THE THESIS

- **Deniz KAVRAR**, M.Lütfi ÖVEÇOĞLU, Halit S.TÜRKMEN.(13-16 July 2011) Production of a Helicopter Tail Boom and Associated Mechanical Tests. *Advances in Materials and Processing Technologies* 2011 İstanbul. (AMPT2011).
- **Deniz KAVRAR**, M.Lütfi ÖVEÇOĞLU, Halit S.TÜRKMEN. (24-28June 2012) Production and Mechanical Testing of the Unmanned Helicopter Tail Cone. *European Congress on Composite Materials* in Venice (ECCM15)